

Land-Atmosphere Interactions Exacerbated the Drought and Heatwave over Northern Europe during Summer 2018

Paul A Dirmeyer¹, Gianpaolo Balsamo², Eleanor Blyth³, Ross Morrison⁴, and Hollie Cooper⁵

¹George Mason University

²ECMWF Model Division/Physics

³UK Centre for Ecology and Hydrology

⁴Centre for Ecology and Hydrology

⁵UK Centre for Ecology & Hydrology

November 26, 2022

Abstract

The 2018 drought and heatwave over Europe was exceptional over northern Europe, with unprecedented forest fires in Sweden, searing heat in Germany and water restrictions in England. Monthly, daily and hourly data from ERA5, verified with soil moisture and surface flux measurements over Britain, are examined to investigate the subseasonal-to-seasonal progression of the event and the diurnal evolution of tropospheric profiles to quantify the anomalous land surface contribution to heat and drought. Data suggest the region entered a rare condition of becoming a “hot spot” for land-atmosphere coupling, which exacerbated the heatwave across much of northern Europe. Land-atmosphere feedbacks were prompted by unusually low soil moisture over wide areas, which generated moisture limitations on surface latent heat fluxes, suppressing cloud formation, increasing surface net radiation and driving temperatures higher during several multi-week episodes of extreme heat. We find consistent evidence in field data and reanalysis of a breakpoint threshold of soil moisture at most locations, below which surface fluxes and daily maximum temperatures become hypersensitive to declining soil moisture. Similar recent heatwaves over various parts of Europe in 2003, 2010 and 2019, combined with dire climate change projections, suggest such events could be on the increase. Land-atmosphere feedbacks may play an increasingly important role in exacerbating extremes, but could also contribute to their predictability on subseasonal time scales.

**Land-Atmosphere Interactions Exacerbated the Drought and Heatwave over Northern Europe
during Summer 2018**

Paul A. Dirmeyer

Center for Ocean-Land-Atmosphere Studies, George Mason University, Fairfax, Virginia, USA

Gianpaolo Balsamo

European Centre for Medium-range Weather Forecasts, Reading, United Kingdom

Eleanor M. Blyth, Ross Morrison, and Hollie M. Cooper

UK Centre for Ecology and Hydrology, Wallingford, United Kingdom

1 **Abstract**

2 The 2018 drought and heatwave over Europe was exceptional over northern Europe, with
3 unprecedented forest fires in Sweden, searing heat in Germany and water restrictions in England.
4 Monthly, daily and hourly data from ERA5, verified with *in situ* soil moisture and surface flux
5 measurements over Britain, are examined to investigate the subseasonal-to-seasonal
6 progression of the event and the diurnal evolution of tropospheric profiles to quantify the
7 anomalous land surface contribution to heat and drought. Data suggest the region entered a rare
8 condition of becoming a “hot spot” for land-atmosphere coupling, which exacerbated the
9 heatwave across much of northern Europe. Land-atmosphere feedbacks were prompted by
10 unusually low soil moisture over wide areas, which generated moisture limitations on surface
11 latent heat fluxes, suppressing cloud formation, increasing surface net radiation and driving
12 temperatures higher during several multi-week episodes of extreme heat. We find consistent
13 evidence in field data and reanalysis of a breakpoint threshold of soil moisture at most locations,
14 below which surface fluxes and daily maximum temperatures become hypersensitive to declining
15 soil moisture. Similar recent heatwaves over various parts of Europe in 2003, 2010 and 2019,
16 combined with dire climate change projections, suggest such events could be on the increase.
17 Land-atmosphere feedbacks may play an increasingly important role in exacerbating extremes,
18 but could also contribute to their predictability on subseasonal time scales.

19

20 **Plain Language Summary**

21 This study uses a combination of environmental observations over Britain, atmospheric and land
22 surface analyses over Europe to examine the exceptional drought and heatwave over northern
23 Europe during the summer of 2018. Results suggest the region entered a state of positive
24 feedback between the land and atmosphere, exacerbating the heatwave over the area. This is a
25 situation that is common over southern Europe and many other places in the world, but rare for
26 northern Europe. Dry soils and vegetation led to reduced evaporation, increased heating of the
27 surface, warming and drying of the air, contributing to less cloud cover. Particularly, a breakpoint
28 value of soil moisture has been found for most locations, below which evaporation, heating and
29 daily maximum temperatures become significantly more sensitive to declining soil moisture. This
30 is both a worrying indicator for the region in a warming climate and a potential source of
31 additional predictability for the intensification of future heatwave events.

32

34 1. Introduction

35 The summer of 2018 saw a combination of drought and heat concentrated on northern Europe.
36 The conditions had far-reaching economic and ecological impacts, with spring and summer
37 dryness affecting crops and natural vegetation, increased tree and forest mortality, including
38 unprecedented wildfires particularly in Sweden (Clément Albergel et al., 2019; Rösner et al.,
39 2019). The atmospheric circulation began to establish conditions for anomalous heat and drought
40 in the spring, with blocking high pressure and unfavorable moisture sources for precipitation
41 beginning in April (Rösner et al., 2019). European heatwaves are associated with such mid-
42 latitude quasi-stationary wave patterns (Wolf et al., 2016), but advection can also play a
43 significant role (Sousa et al., 2019). Synoptic features of the heatwave were well forecast up to
44 two weeks in advance, and some aspects were evident out to four weeks (Magnusson et al.,
45 2018), suggesting its origins were in the large-scale hemispheric circulation (Kornhuber et al.,
46 2019).

47 The combined hot and dry conditions experienced in northern Europe are more typical of
48 southern Europe, but such situations are projected to become more common in a changing
49 climate (Samaniego et al., 2018; Teuling, 2018; Zscheischler et al., 2018). For example, the
50 summer of 2018 was among the warmest, sunniest and driest on record in the UK (Kendon et al.,
51 2019). A regional modeling study has suggested some of the heatwave signal over Britain may be
52 attributable to the effect of regional sea surface temperature anomalies (Petch et al., 2020). The
53 same study suggests local soil moisture anomalies had nearly as large an impact on temperatures.
54 Northern Europe is not a region which typically experiences land-atmosphere coupling that
55 promotes positive feedbacks in situations such as droughts or heatwaves (Seneviratne et al.,
56 2010). Could it be that northern Europe entered into an unprecedented positive feedback regime
57 during the summer of 2018?

58 There is generally a positive relationship between soil dryness and heat (Fischer et al., 2007;
59 Hirsch et al., 2014; Philip et al., 2018; Santanello et al., 2011). Obviously high temperatures are
60 conducive to drying the soil by increasing the evaporative demand by the atmosphere. But there
61 is a positive feedback – dry soils heat more quickly than wet ones and may thus transmit absorbed
62 radiant energy to the atmosphere as sensible heat more readily than wet soils, as the gradient
63 between surface and near-surface air temperatures can become larger. Furthermore, dry soils
64 correspond to reduced evaporation, and if dry enough to sufficient depth, reduced transpiration
65 by plants. This reduces evaporative cooling potentially further exacerbating the heat (Dirmeyer
66 et al., 2015). In general, land surface states and soil moisture can be a source of such feedbacks
67 when water availability in the soil is a limiting or controlling factor for evapotranspiration, while
68 the land is not a factor in energy-limited situations such as when conditions are wet, cool and
69 cloudy (Santanello et al., 2018).

70 It is through the processes that permit soil moisture variations to affect surface heat fluxes and
71 near-surface meteorological states that land surface feedbacks to the atmosphere occur
72 (Dirmeyer, Gentine, et al., 2018). The feedbacks also alter the daytime boundary layer, which can
73 ultimately affect cloud formation, precipitation, and the state of the free atmosphere above the
74 boundary layer (Santanello et al., 2011). When and where there is atmospheric sensitivity and
75 responsiveness to changes in the land state, the land becomes a source of predictability for the
76 atmosphere, a “hot spot” of land-atmosphere coupling (Koster et al., 2006). In the case of
77 droughts and heatwaves, the land surface can be a source of persistence and intensification of
78 the extreme states (Miralles et al., 2018). These effects are most important when radiative
79 energy is most abundant. In mid-latitudes this is during late spring and summer, and diurnally it
80 is during the daylight hours. The diurnal evolution of the atmospheric boundary layer over land
81 is driven by sensible heating of the atmosphere from contact with the surface (Santanello et al.,
82 2009). Many past studies have concentrated on the daylight hours and processes active at that
83 time (Betts, 2004; Ek & Holtslag, 2004; Gentine et al., 2013; Santanello et al., 2007; Zhang et al.,
84 2020). Adequate temporal resolution of the diurnal cycle is key for such studies.

85 Over Europe, recent years have seen several episodes of unprecedented heat (Russo et al., 2015),
86 and future climate projections strongly suggest a positive trend for such events (Lau & Nath,
87 2014; Seneviratne et al., 2006). Over northern Europe there is particular concern, as there is little
88 history of such events. Although warning systems are being implemented, infrastructure is not
89 designed or well prepared to cope with heatwaves (Casanueva et al., 2019; Lass et al., 2011).
90 Drought has also been a much more common event in southern Europe than northern Europe
91 (Vicente-Serrano et al., 2014). While positive trends in drought are indicated in both regions, with
92 drying common to majority of land areas (Albergel et al., 2013) the unfamiliarity with such
93 extremes in the North introduces additional challenges.

94 Modeling studies indicate that most of northern Europe is usually in an energy-limited regime,
95 even during the warmer summer months, and thus not responsive to soil moisture anomalies
96 (Dirmeyer et al., 2009; Schwingshackl et al., 2018). This is because there is a range of soil moisture
97 over which a fairly linear and decidedly monotonic relationship exists with latent heat fluxes.
98 Above a certain value of soil moisture, the dependence of latent heat on soil moisture diminishes
99 or disappears. Likewise, there is a lower bound of soil moisture below which latent heat flux shuts
100 down. These thresholds are often associated with the field capacity and wilting point
101 respectively, although latent heat flux may fail to increase with increasing soil moisture below
102 field capacity if insufficient net radiation is available to drive maximum evapotranspiration – this
103 is often the case in northern Europe.

104 Given the concurrent dry and warm conditions over much of northern Europe during the summer
105 of 2018, we pose the question: Did northern Europe enter a regime of land surface feedbacks to
106 the atmosphere – i.e., did it become a “hot spot” that may have intensified the heatwave? We

107 combine analysis of *in situ* observational data and state-of-the-art gridded reanalyses to
108 investigate the question. Section 2 describes the data used. Analysis techniques and metrics of
109 land-atmosphere interaction are presented in Section 3. Results are shown in Section 4, followed
110 by conclusions in Section 5.

111

112 **2. Data**

113 Hourly data from the European Centre for Medium-range Weather Forecasts (ECMWF) ERA5
114 covering the 40-year period 1979-2018 are used in this study (Hersbach et al., 2020). The data
115 are at a nominal 31 km resolution but have been interpolated back to the full TL639 grid (~0.28°)
116 for this analysis. Vertical resolution is also higher than any previous reanalysis, with 23 layers in
117 the lowest 15% of the atmosphere by mass, and 55 layers in the lowest 70%.

118 ERA5 is the first reanalysis to assimilate satellite soil moisture data (de Rosnay et al., 2014). This
119 assures better quality analyses of soil moisture, but also assures a lack of closure of the terrestrial
120 water balance. Nevertheless, reanalyses have been shown to perform well in regard to the
121 simulation of land-atmosphere coupling metrics based on daily data (Dirmeyer, Chen, et al.,
122 2018). ERA5 provides the opportunity to examine the diurnal cycle with unprecedented detail as
123 hourly data for all atmosphere and land surface variables are available. The diurnal cycle is a key
124 element of coupled land-atmosphere processes (Santanello et al., 2018). The 12-hour data
125 assimilation windows are shifted 6 hours from the 0000 and 1200UTC windows used in previous
126 reanalyses, and artifacts are sometimes evident toward the end of those windows, as is shown
127 in Section 4. Note that because of lack of local budget closure in the reanalysis fields, exact
128 budgets cannot be calculated. Nevertheless, a good depiction of the temporal variability in
129 budget terms is afforded.

130

131 For *in situ* analysis and comparisons over Britain, data from two grassland flux towers in southern
132 England operated by the UK Centre for Ecology and Hydrology (UKCEH) are used. The eddy
133 covariance instrumentation combines Gill Instruments Ltd. (Lymington, UK) ultrasonic
134 anemometer-thermometers and LI7500 series infrared gas analyzers (Li-COR Biosciences,
135 Nebraska, USA), alongside a standardized set of micrometeorological (radiation, air temperature,
136 humidity and pressure) and soil physics (temperature, moisture and heat flux) sensors. Data
137 processing and quality control follow methods of the global flux measurement community
138 (Fratini & Mauder, 2014; Papale et al., 2006; Reichstein et al., 2005). Full details of the
139 measurement sites, instrumentation and data handling can be downloaded with the eddy
140 covariance datasets (Morrison et al., 2019, 2020). The data duration is short compared to ERA5,
141 but provides ground truth to validate aspects of the coupled land-atmosphere behavior in ERA5
142 – fidelity lends confidence to the larger-scale analyses. As with ERA5, energy and water budgets

143 from the eddy covariance sites do not close, but well-managed flux tower sites can still have great
144 value for assessing local heatwave maintenance processes (Horst et al., 2019).

145 UKCEH also maintains a network of large-area soil moisture monitoring sites (COSMOS-UK), with
146 collocated meteorological observations, that is based on the cosmic ray neutron sensor. The
147 COSMOS-UK network has been developed since 2013 and provides sub-daily field scale soil
148 moisture, derived from fast neutron counts at the land surface (Stanley et al., 2019). Near surface
149 soil moisture is determined using corrections for local atmospheric pressure, humidity and
150 background neutron intensity (Evans et al., 2016; Rosolem et al., 2013), and site-specific
151 calibration based on destructive soil sampling (Evans et al., 2016). The COSMOS-UK network is
152 more extensive than the flux towers, providing a distributed picture of near-surface water
153 storage over Britain. Figure 1 provides a map of all site locations used in this analysis (Antoniou
154 et al., 2019). Additionally, surface fluxes have been estimated for some COSMOS-UK sites; where
155 sensible heat flux is derived from eddy covariance instrumentation, and latent heat flux
156 estimated as a residual from the other terms of the surface energy budget measured at COSMOS-
157 UK sites (Crowhurst et al., 2019).

158 Such *in situ* measurements provide ground truth at a small number of locations around Britain,
159 which are used to validate the behavior of ERA5 data that provide complete coverage over the
160 entire domain of interest. Tables S1 and S2 show the temporal correlations of daily time series
161 between observations and ERA5 for soil water content and daily maximum temperature at the
162 COSMOS-UK sites, and for a number of variables at the flux tower sites. Correlations are
163 calculated separately for 2017 and 2018 for the warm season period spanning 15 May through
164 15 October – a period of 154 days. In every case, the correlations are significant at the 99%
165 confidence level, suggesting ERA5 provides a trustworthy univariate representation of states and
166 fluxes near the surface. Multivariate behavior, which is a crucial indicator of processes linking
167 land and atmosphere, is the topic of study in results section.

168

169 **3. Metrics**

170 In order to investigate the possible role of land-atmosphere feedbacks on the 2018 heatwave
171 and drought, we estimate several land-atmosphere coupling metrics as well as energy budget
172 terms over affected areas. Anomalies in temperature, volumetric soil water content, and fluxes
173 are calculated relative to a 40-year (1979-2018) climatological period for ERA5 data. For *in situ*
174 data over Britain, comparisons between corresponding periods in 2018 and 2017 are made, as
175 long records are not available from the relatively new networks.

176 Daily data are used to produce areal averages of key heat and moisture budget terms averaged
177 over selected regions. Surface and atmospheric budgets are produced on an hourly timescale
178 averaged over Britain to derive mean diurnal cycles of surface and vertical heating profiles. The

179 ERA5 land mask is used to define the areal domains as land grid cells only, and averages across
180 the grid cells are area weighted. For the vertical profiles of atmospheric variables, calculations
181 are performed on the native ERA5 vertical levels, whose thicknesses at any location are
182 proportional to surface pressure (i.e., a sigma coordinate in the vertical). The vertical dimension
183 over Britain is rendered in the model coordinate as values relative to a surface pressure of
184 1013.25 hPa, but are in fact usually somewhat smaller, especially over elevated terrain.

185 Lifted condensation level (LCL) is compared to the depth of the planetary boundary layer (PBL)
186 to determine an LCL deficit (Santanello et al., 2011). We define it here with the opposite sign
187 from its original specification, such that negative values indicate the PBL does not grow deep
188 enough for condensation and cloud formation to occur at its top. Such a shortfall can be caused
189 by either insufficient heating at the surface to generate the necessary buoyancy, low relative
190 humidity of air near the surface, or a combination of both.

191 Segmented regression is used to determine if there is a significant change in the relationship
192 between soil moisture and extreme temperatures or surface fluxes that can be attributed to land-
193 atmosphere feedbacks (Wu & Dirmeyer, 2020). Figure 2 provides an example at one ERA5 grid
194 cell: for a specific time period (in this case a particular calendar month across 40 years), daily
195 values of surface (0-7 cm) volumetric soil moisture and daily maximum air temperature are seen
196 to have an inverse relationship, which is typical of many mid-latitude locations. To determine
197 whether there is a difference in the slope of temperature estimated over different ranges of soil
198 moisture, an optimization is calculated to minimize the RMS error of a pair of linear regressions
199 over two segments which together cover the entire range of soil moisture at that grid cell and
200 month (V. M. Muggeo & Hajat, 2009; V. M. R. Muggeo, 2003). The criterion is that the two linear
201 regressions must intersect at the same value of temperature (red dot) at the soil moisture
202 breakpoint between the segments (red line). Optimization is performed over four parameters:
203 the slopes of the left (drier) and right (wetter) segments, the breakpoint values of soil moisture
204 and maximum temperature.

205 Additional criteria are applied to filter the results. First, the two slopes must be significantly
206 different. The variances of the estimates of the two slopes are averaged after adjusting down the
207 sample size of N days by the soil moisture memory τ in days as $N/(\tau + 1)$, to properly account
208 for the degrees of freedom. From that, a z-score and p-score are calculated assuming a normal
209 distribution of the potential errors in parameter estimates; p-scores of 0.01 or less are retained.
210 Because we have in mind specific physical processes by which low soil moisture may affect air
211 temperature, we further constrain that the slope of the linear regression to the left of the
212 estimated breakpoint be negative for temperature or sensible heat flux, positive for latent heat
213 flux or evaporative fraction, and that the slope have a larger magnitude on the drier side of the
214 breakpoint than the wetter side. We also check that there are at least 10 data points on either
215 side of the breakpoint. Locations where the optimization fails to converge are omitted.

216

217 **4. Results**

218 A question emerges for the summer of 2018: did locations in northern Europe move into a regime
219 where land surface feedbacks exacerbated drying and warming? First, the degree of the
220 extremities for summer 2018 are determined. Figure 3 shows the fraction of the 122 days of May
221 through August 2018 that lie within the indicated tails of maximum 2m air temperature
222 anomalies and surface (top 7 cm) volumetric soil water content, based on ERA5. By chance, one
223 would expect a value of 0.05 at any location in the maximum temperature plot, and 0.25 for soil
224 water content. There is strong spatial correspondence between the two panels, but the core or
225 dry soils is clearly south of the core of high temperatures. In parts of Germany, nearly every day
226 of May-August 2018 are in the driest quartile. For temperature, the most extreme conditions
227 were over southern Scandinavia, where up to one third of the period was in the warmest 5% of
228 anomalies of the previous 40 years. Each panel shows large areal coverage of significant
229 anomalies, yet much of Eastern Europe is significantly dry but not significantly warm.

230 The evolution of monthly mean anomalies in surface volumetric soil moisture and maximum 2 m
231 air temperature over land are shown in Figure 4 for the period of May-August 2018. Anomalously
232 warm and dry conditions predominate over northern Europe in each month, but the patterns are
233 not stationary. For soil moisture, only areas around northern Germany and the Baltic states are
234 more than 0.03 drier than average in every month. Areas of positive temperature anomalies
235 alternate between extreme heat over Scandinavia and lands adjacent to the North and Baltic seas
236 (May, July) and less intense but still widespread warm anomalies anchored around Germany
237 (June, August).

238 A more complete picture is given in supplemental figures Figures S1-S3, which portray anomalies
239 in boundary layer states, surface energy and moisture fluxes as represented in ERA5.
240 Precipitation and soil moisture evolve similarly, while anomalies in surface turbulent heat fluxes
241 are much more prominent in sensible than latent heat flux (Figure S1). Increases in sensible heat
242 flux correspond strongly with positive anomalies in downward shortwave radiation (Figure S2).
243 Meanwhile, latent heat flux deficits are more closely linked to extremely dry soil, particularly
244 during July and August. The planetary boundary tends to be slightly deeper in most regions
245 (Figure S3) but is outpaced by the increases in the lifted condensation level, hampering cloud
246 formation in areas where downward shortwave radiation increases.

247 There was considerable synoptic variability in heatwave and drought conditions during 2018 and
248 the use of monthly means does not capture the nuances nor the peak periods. Nevertheless, the
249 preceding figures give a good first-order impression of the magnitude and duration of warm dry
250 conditions over northern Europe during the period.

251 Focusing on three areas that bore the brunt of the hot conditions: Southern Scandinavia
252 (hereafter SSc), the Northern European Plain (NEP) and the island of Britain (all outlined in Figure
253 3), Figure 5 presents area averages of daily time series during May-August. The top row shows
254 volumetric surface soil moisture for 2018 relative to its 40-year (1979-2018) climatological
255 evolution, simply calculated as daily means with a centered 7-day running average applied. Each
256 region was predominantly drier than normal, with the greatest anomalies during the first half of
257 July. SSc also had a dry period during late May and early June that was as intense as during July,
258 while NEP also saw very dry conditions in late July and August. Britain's driest period spanned
259 from late June to late July. The second row shows the climatological and 2018 accumulated
260 precipitation from 1 May onwards, showing extreme shortfalls in all regions, although both SSc
261 and Britain showed rainfall rates returning to normal in August (matching slopes of the curves).

262 Area averaged daily maximum temperatures are shown in the middle row of Figure 5. Positive
263 anomalies dominate in all regions. Heatwave peaks correspond largely to the periods of lowest
264 soil moisture except over NEP where the late May heat was during a period clearly wetter than
265 the early July dry period during which temperatures were mainly 1-5°C above average rather than
266 8-10°C. The fourth row shows the LCL deficit (Santanello et al., 2011): negative values indicate
267 the boundary layer does not grow deep enough for condensation and cloud formation to occur.
268 The climatological lines show deficits hovering around 0 m over SSc and NEP, and consistent
269 positive values over Britain suggesting clouds are likely to form above a growing boundary layer
270 during every day of the period. During 2018, deficits predominate over SSc and NEP, as well as
271 during the most intense heatwave periods over Britain, where summer values were usually well
272 below climatology. From Figure S3 it can be seen that the main cause was elevated LCL heights
273 due to warm dry air, as PBL growth was not suppressed markedly during the period and was often
274 above average.

275 The periods lacking convective clouds over land correspond to anomalous increases in downward
276 shortwave radiation at the surface (Figure 5, bottom row). Those are also periods of enhanced
277 sensible heat flux in ERA5, but latent heat flux is not as responsive to the fluctuations in radiation.
278 In fact, an interesting reversal occurs around July 1. Before that period, latent heat flux is clearly
279 positively correlated with shortwave radiation, suggesting evaporation is limited by available
280 energy. This is the typical situation across northern Europe. After 1 July, latent heat flux becomes
281 anticorrelated with both shortwave radiation and sensible heat flux, indicative of a moisture-
282 limited situation. This is a necessary condition for land-atmosphere feedback (Dirmeyer et al.,
283 2015), suggesting a rare and possibly unprecedented situation of the development of a coupling
284 "hot spot" from land to atmosphere that may have exacerbated the heatwave.

285 To better establish the linkages between soil moisture and temperature extremes over Europe,
286 we have applied the segmented regression analysis described in Section 3 to the ERA5 soil
287 moisture and maximum temperature data across northern Europe for the 1979-2018 period to

288 estimate a climatology of breakpoint statistics. Monthly results are shown in Figure 6. The
289 estimated breakpoint between two linear regressions is only shown where the criteria outlined
290 in Section 3 are met. Of all the grid cells in the domain, the number shaded rises from 51% in May
291 to nearly 70% in July. The segmented regression calculation fails to converge for between 1-2%
292 of cells, and only 2-3% of cells fail to pass the significance test even with the degrees of freedom
293 reduced in proportion to the soil moisture memory timescale. The most common criterion to be
294 failed is that the change in slope is not more negative on the dry side of the breakpoint – this
295 happens for 45% of land grid cells in May, dropping to under 28% in July.

296 Despite passing these criteria, many points do not conform to our process-based expectation for
297 soil moisture control of temperature in moisture-limited, energy-abundant situations. The
298 breakpoint is shown both in units of volumetric soil moisture (Figure 6 left column) and as a
299 normalized 0-1 index whose range is bounded by the lowest and highest daily soil moisture values
300 registered in 40 years of ERA data for the month (middle column). It is clear from the index values
301 that breakpoints in the higher range of local soil moisture (bluer colors) correspond with smaller
302 changes in slope (yellow colors in the right column). This situation is persistent over much of
303 Scandinavia and the British Isles, indicating that extremely warm and dry conditions are too rare
304 to influence detection of a breakpoint toward the dry end of the range. In fact, the widespread
305 areas of wet breakpoints paired with large slope changes over northern Scandinavia during May
306 are associated with snowmelt and thawing ground within a moist, energy-limited environment
307 rather than a heatwave feedback process. On the other hand, dry values for breakpoints paired
308 with major changes in slope are common in all months across most of southern Europe and
309 emerge in parts of the Northern European Plain and Eastern Europe during July and August. The
310 large change in slope is indicative of a hypersensitive realm at very low soil moistures where
311 daytime temperatures can elevate markedly as soil dries.

312 The relationship among the soil moisture breakpoint, change in slope $\frac{dT_{Max}}{dSM}$, surface fluxes and
313 the strength of land-atmosphere coupling can be seen clearly in Figure 7. The correlation
314 between latent heat flux and soil moisture is the main component of the terrestrial coupling
315 index (Dirmeyer 2011), indicating strength of feedback of land surface states onto the lower
316 troposphere. The L-shaped distribution in the left panel shows that strong coupling is associated
317 with locations where the breakpoint occurs at relatively dry soil moisture. These also tend to be
318 locations with abundant sensible heat flux, mostly in Southern Europe (right panel), indicative of
319 a shutdown of evapotranspiration consistent with the theory described earlier. Locations with
320 very low sensible heat flux, regardless of the estimated value of the breakpoint, have weak
321 correlation or anti-correlation between latent heat flux and soil moisture, indicating that they
322 are not moisture-limited locations where soil moisture content typically regulates surface flux
323 partitioning. The breakpoint algorithm almost always finds a statistically significant change in

324 slope, given such a large sample size, but often over Europe it is not indicative of a physical
325 mechanism whereby the land surface control of atmospheric states is enhanced in dry conditions.

326 To attempt to verify the bivariate relationships related to land-atmosphere coupling shown so
327 far using ERA5 data, we focus on Britain due to the availability of *in situ* soil moisture,
328 meteorological and flux data. If we find that the observed relationships between links in the
329 process chain of land-atmosphere coupling (Santanello et al., 2018) are represented well in ERA5
330 over Britain, we may use the reanalyses to extrapolate conclusions to the rest of northern Europe
331 with greater confidence.

332 Figure 8 provides a diurnal Hovmöller diagram of the vertical profile of diabatic heating from
333 ERA5, averaged over the land grid cells of the Britain box shown in Figure 3. The mean warm-
334 season diurnal profile for the 39 years prior to 2018 shows the warming and deepening of the
335 boundary layer from sunrise through the afternoon, with shallow cooling at night.
336 Climatologically, there is convective warming that breaks through the boundary layer in the late
337 afternoon, leading to enhanced mid-tropospheric warming due to latent heat release. In fact,
338 there is weak warming in the mid-troposphere at all times of day due to frequent clouds.
339 Climatologically the boundary layer height is above the lifted condensation level (LCL), another
340 indication that Britain is more often cloudy than not. Peak surface sensible heat flux occurs an
341 hour after noon at just over 100 Wm^{-2} . In 2018 daytime boundary layer heating is stronger during
342 the day and cooling is weaker at night. There is less heating of the troposphere above the
343 boundary layer due to less latent heat release from reduced cloudiness. There is actually net
344 cooling above the boundary layer from mid-morning to mid-afternoon due to entrainment of
345 lower potential temperature air from below becoming dominant given the lack of cloud
346 formation. The LCL is higher while boundary layer depth is lower, and surface sensible heat flux
347 is about 20% greater. Figure S4 presents a similar analysis for moisture fluxes – the anomalies at
348 08 and 20 UTC are artifacts of the data assimilation cycle, but otherwise more aggressive heating
349 of the boundary layer appears to lead to stronger moisture diffusion and entrainment into the
350 free atmosphere without condensation, but stronger nighttime drying of the lower troposphere
351 and little change in surface latent heat flux.

352 Breakpoint analyses in the manner of Figure 2 are shown in Figure 9 for ten COSMOS-UK sites
353 that have complete soil moisture and meteorological data for the summers of 2017 and 2018.
354 The heatwave year of 2018 (red) shows a significant regression slope on the dry side of the
355 breakpoint at every station that is steeper than on the wet side of the breakpoint, and in better
356 agreement with the two-year estimate (green) than is the 2017 regression (blue). The soil
357 moisture breakpoint values for 2018 are also more stable and in better agreement with the 2-
358 year estimate than are the 2017-based values. 2017 slopes are often not significant and for
359 several stations do not conform to the theory of dry soils driving higher temperature, likely
360 because the 2017 sample does not contain many or any hot dry days typical of a land-atmosphere

361 feedback. Figure 10 shows the same analysis for the ERA5 grid cells containing the COSMOS-UK
362 sites. ERA5 estimates consistently show a shallower slope on the dry side of the breakpoint,
363 indicating less sensitivity of daily maximum temperatures to drying soils than observations, and
364 less of a change in slope (sensitivity) between the wet and dry sides of the breakpoint. The
365 breakpoint algorithm struggles to find significant changes at some locations, like Hartwood Home
366 and Riseholme where there is a clear signal in 2018 for the COSMOS-UK data but for neither year
367 in ERA5. Overall it appears that ERA5 underestimates the impact of very dry soils on extreme
368 temperatures, at least over Britain. A reason for the lower coupling to drought/Tmax in ERA5
369 might be the lack of soil moisture-vegetation feedback, since ERA5 adopts a monthly climatology
370 of leaf area index (Boussetta et al., 2013). Moreover, recent findings by Nogueira et al. (2020)
371 highlight the interplay of vegetation cover and state in further enhancing surface temperatures.

372 Figure S5 compares the results from Figures 9 and 10 for four categories of breakpoint statistics.
373 Compared to the ten COSMOS sites, ERA5 consistently overestimates the volumetric soil water
374 content at the breakpoint, underestimates the sensitivity of daily maximum temperature to
375 drying soils, and overestimates the correlation between maximum temperature and soil moisture
376 on the dry side of the breakpoint. ERA5 also gives a very uniform difference between 2018 and
377 2017, showing 30-45% more dry days in 2018, while COSMOS observations show a wider range
378 from 10-56% increases for 2018. Most of these discrepancies could be explained by the differing
379 natures of point measurements versus model grid cell estimates. Model data contains no
380 observational error, so the higher regression correlations for ERA5 are to be expected as there is
381 no random error to degrade correlations. Reduced sensitivity in ERA5 may be attributed to the
382 large spatial area of a model grid cell, nearly 10^3 km², muting variability and causing all of the
383 blue linear-fit lines to be flatter than the 1:1 red dotted line. This may also explain the uniformity
384 in the difference between 2018 and 2017 dry days, as local variations in rainfall and hillslope
385 properties that affect local soil moisture are not resolved in ERA5. However, the systematic
386 overestimation by ERA5 of soil water content at the breakpoint suggests a bias in model soil
387 parameters or perhaps model physics. The only significant inter-station correlation found
388 between ERA5 and COSMOS is for the magnitude of the correlation on the dry side of the
389 breakpoint (shown in green), although all are positively correlated.

390 There are fewer flux towers than COSMOS-UK sites that have data necessary to assess breakpoint
391 relationships between surface fluxes and soil moisture. The Great Fen site has time domain
392 transmissometry (TDT) soil moisture sensors only (surface layer data are used), while Sheepdrove
393 is also a COSMOS-UK site. Breakpoint analysis of evaporative fraction (EF) versus volumetric soil
394 water content for these stations is shown in Figure 11; Figures S6 and S7 show results separately
395 for sensible and latent heat fluxes. At Sheepdrove, the soil moisture breakpoints estimated
396 independently using EF and maximum air temperature (Figure 11) are within 1% of each other
397 for the two years combined, suggesting a mechanistic link between soil moisture and extreme

398 temperature via surface heat flux partitioning. As with previous figures, the flux-based results are
399 less representative and robust for 2017, although at Great Fen there are significant dry-side
400 sensitivities for both years that are very similar to each other.

401 The same analysis with ERA5 (right panels) differs systematically from the flux tower analysis. In
402 ERA5, there appears to be too much sensitivity of EF to soil moisture variations when soils are
403 wet (greater positive slope). The field sites show EF values consistently centering on 0.8 on the
404 wet side of the breakpoint, whereas ERA5 ranges from 0.9 down to 0.7 at the breakpoint. ERA5
405 also shows much less sensitivity on the dry side of the breakpoint (compare slope values in the
406 green boxes). In other words, the break is much clearer in observations than the reanalysis. ERA5
407 grid cells represent an area average, so it may actually characterize the net distribution of
408 heterogeneous drydowns and their effect on fluxes rather well. That cannot be discerned from
409 this analysis, but this comparison to point data at flux towers shows stark differences. At both
410 sites during the drought, EF attains lower daily values of EF than does ERA5. Examination of
411 sensible and latent heat fluxes separately (Figures S6 and S7) show that in all cases, most of the
412 signal in evaporative fraction comes from the sensible heat flux, and the contrast in distributions
413 on either side of the estimated breakpoints is always starker in observations than in ERA5.
414 Nevertheless, ERA5 does reproduce the overall signature of increasing sensitivity of surface fluxes
415 to soil moisture as soils dry below a critical point.

416 Some of the COSMOS-UK sites have eddy covariance estimates of sensible heat flux and the
417 necessary radiation and ground heat flux measurements to estimate latent heat flux as a residual
418 for 2017 and 2018. The estimated breakpoints for sensible heat flux and EF at those six sites are
419 shown in Figure 12. At every site, there is a significant detection of a breakpoint for sensible heat
420 flux and significantly sharper increases over drier soils. For evaporative fraction, the relationships
421 are slightly less clear, consistent with the weaker role of soil moisture controls on latent heat flux
422 suggested in Figures S6, S7 and 11. Although not apparent to the eye, the change in slope for EF
423 at Redhill is significant but the position of the breakpoint is unreliable, indicated by the grey oval
424 of uncertainty. Porton Down is similarly uncertain for EF, and the change in slope across the
425 breakpoint is not of the expected sign. However, in each case, the correlation of the linear
426 regression on the dry side of the breakpoint is stronger than on the wet side, suggesting increased
427 control of soil moisture over surface fluxes as drought sets in. Furthermore, the values of
428 volumetric soil water content of the breakpoints calculated at each station using either EF,
429 sensible heat flux or evaporative fraction are much closer together than are the average
430 breakpoint values among stations. This is true for in situ data and ERA5 grid cells containing the
431 stations. 91% of the total variance in breakpoint soil moisture values in observations is due to
432 inter-station variance; for ERA5 data it is 86%. The remaining variance is the small disagreements
433 between estimates using maximum temperature or different surface fluxes. Furthermore, at
434 every location for every variable in either source of data, the correlation of the linear regression

435 on the dry side of the breakpoint is greater and more significant than on the wet side. All these
436 results suggest a real physical link between declining soil moisture, flux anomalies and extreme
437 heat.

438 The comparison of ERA5 to field observations over Britain provides context to interpret
439 continental maps of drought – heatwave breakpoint statistics. We find that just as with Figure 6,
440 European maps of EF breakpoint statistics are quite stable from month to month (Figure S8) and
441 the spatial patterns of breakpoints are very consistent between EF and maximum temperature.
442 Table 1 shows the degree to which soil moisture breakpoint values calculated with surface fluxes
443 from ERA5 agree with maximum temperature-based breakpoint estimates. Differences are quite
444 small between breakpoints estimated with any variable except latent heat flux, which shows a
445 strong positive bias (breakpoint occurring at a higher value of soil water content) and root mean
446 square errors 15-45% higher than other flux variables. The relationship between soil water
447 content and sensible heat flux appears to be the controlling factor for temperature sensitivity
448 amplification during combined drought heatwave cases, supporting in a temporal sense the
449 result suggested spatially in Figure 7.

450 Finally, the fraction of days during May through August 2018 that lie on the dry side of the
451 climatologically estimate breakpoints based on both maximum temperature and evaporative
452 fraction are shown in Figure 13. In each case, the climatological fraction of days is subtracted, so
453 that positive values suggest more days than average in the hypersensitive soil moisture regime
454 during 2018. Comparison to Figure 3 shows how this metric synthesizes the extremes in soil water
455 content and temperature, as well as providing a spatial depiction of regions where land-
456 atmosphere feedbacks could have exacerbated the hot conditions in 2018. Large portions of
457 northern Europe experienced at least a 25% increase in the number of critically dry soil days,
458 including not only the three regions highlighted earlier in the study, but also over large areas of
459 the eastern Baltic and western Eurasian steppes. Very few areas had a decrease in the number
460 of critically dry days during the warm season of 2018.

461

462 **5. Conclusions**

463 In this study, we have used a combination of high-quality reanalyses and *in situ* measurements
464 of volumetric soil water content, temperature and surface fluxes to demonstrate the existence
465 of a breakpoint in the range of soil water content below which the sensitivity of the atmosphere
466 to drying soils substantially increases, providing a potential positive feedback mechanism by
467 which the land surface may exacerbate heatwaves during drought conditions. Specifically, we
468 diagnose the 2018 drought and heatwave over Northern Europe, an area that rarely enters into
469 classically defined regimes amenable to land-atmosphere feedbacks (Santanello et al., 2018;
470 Seneviratne et al., 2010).

471 During 2018, exceptionally dry conditions spread throughout much of northern Europe in
472 concurrence with multiple prolonged episodes of extreme heat. Segmented regression analysis
473 uninformed by any physical processes has been found to identify stable values of breakpoints in
474 the range of soil water content consistently at most locations, including soil moisture monitoring
475 sites in Britain. The values of soil water content are largely invariant from month to month when
476 calculated on a monthly basis and are also very similar whether the regressions are trained with
477 dependent variable being daily maximum air temperature, sensible heat flux or evaporative
478 fraction. There are greater variations when latent heat flux is the dependent variable, suggesting
479 the loss of evaporative cooling is less of a regulator of extreme heat than the direct warming of
480 desiccated land surfaces and transfer of that heat to the atmosphere.

481 Patterns over Europe in ERA5 data show very broad potential for land-atmosphere feedbacks to
482 have exacerbated the extreme heat during 2018. However, field data over Britain suggest ERA5
483 may underestimate the increase of sensitivity of extreme temperatures to declining soil moisture
484 in very dry conditions, so the European maps based on ERA5 data may not represent the full
485 potential impact of drying soils on heatwaves. The present study cannot establish the degree to
486 which scale differences between the flux tower and COSMOS soil moisture sites (with a footprint
487 no larger than 1 km²) and ERA5 grid cells (around 10³ km²) contribute to the discrepancies. Few
488 areas of Europe were free from dry conditions during the summer of 2018, so a combination of
489 local land-driven feedback mechanisms suggested here and non-local mechanisms (Berg et al.,
490 2016; Miralles et al., 2018; Schumacher et al., 2019) could have contributed to the observed
491 extremes.

492 The consistency of apparent breakpoint thresholds of soil moisture below which surface fluxes
493 and daily maximum temperatures become hypersensitive to declining soil moisture provides a
494 source of predictability for severe heatwaves. Recognition of the role of low soil moisture in
495 exacerbating extreme heat, the correct representation in forecast models of the processes
496 governing the increased sensitivity, and proper initialization of those forecast models with real-
497 time soil moisture conditions will all contribute to increased forecast skill and improved early
498 warning of heatwaves, even in regions which have historically been immune from such extremes.

499

500 *Acknowledgements:*

501 This research is the result of Dr. Dirmeyer's sabbatical visits to the European Centre for Medium-
502 range Weather Forecasts in July 2018 and March-April 2019, hosted by Dr. Balsamo. A portion of
503 this work was supported by the Natural Environment Research Council award number
504 NE/R016429/1 as part of the UK-SCAPE programme delivering National Capability. UKCEH field
505 data are available as indicated through the references provided herein to the Centre's online data
506 catalogue (see: <https://catalogue.ceh.ac.uk/eidc/documents>). The Copernicus Climate Change

507 Service (C3S) provides access to ERA5 data freely through its online portal at:
508 <https://cds.climate.copernicus.eu/cdsapp#!/home>.

509

510

511 **References**

- 512 Albergel, C., Dorigo, W., Reichle, R. H., Balsamo, G., de Rosnay, P., Muñoz-Sabater, J., et al.
513 (2013). Skill and Global Trend Analysis of Soil Moisture from Reanalyses and Microwave
514 Remote Sensing. *Journal of Hydrometeorology*, 14(4), 1259–1277.
515 <https://doi.org/10.1175/JHM-D-12-0161.1>
- 516 Albergel, Clément, Dutra, E., Bonan, B., Zheng, Y., Munier, S., Balsamo, G., et al. (2019).
517 Monitoring and Forecasting the Impact of the 2018 Summer Heatwave on Vegetation.
518 *Remote Sensing*, 11(5), 520. <https://doi.org/10.3390/rs11050520>
- 519 Antoniou, V., Askquith-Ellis, A., Bagnoli, S., Ball, L., Bennett, E., Blake, J., et al. (2019,
520 August 19). COSMOS-UK user guide: users' guide to sites, instruments and available data
521 (version 2.10) [Publication - Report]. Retrieved May 18, 2020, from
522 [https://cosmos.ceh.ac.uk/sites/default/files/COSMOS-](https://cosmos.ceh.ac.uk/sites/default/files/COSMOS-UK%20User%20Guide%20v2.10.pdf)
523 [UK%20User%20Guide%20v2.10.pdf](https://cosmos.ceh.ac.uk/sites/default/files/COSMOS-UK%20User%20Guide%20v2.10.pdf)
- 524 Berg, A., Findell, K., Lintner, B., Giannini, A., Seneviratne, S. I., Hurk, B. van den, et al.
525 (2016). Land–atmosphere feedbacks amplify aridity increase over land under global
526 warming. *Nature Climate Change*, 6(9), 869–874. <https://doi.org/10.1038/nclimate3029>
- 527 Betts, A. K. (2004). Understanding Hydrometeorology Using Global Models. *Bulletin of the*
528 *American Meteorological Society*, 85(11), 1673–1688. [https://doi.org/10.1175/BAMS-85-](https://doi.org/10.1175/BAMS-85-11-1673)
529 [11-1673](https://doi.org/10.1175/BAMS-85-11-1673)
- 530 Boussetta, S., Balsamo, G., Beljaars, A., Kral, T., & Jarlan, L. (2013). Impact of a satellite-
531 derived leaf area index monthly climatology in a global numerical weather prediction
532 model. *International Journal of Remote Sensing*, 34(9–10), 3520–3542.
533 <https://doi.org/10.1080/01431161.2012.716543>
- 534 Casanueva, A., Burgstall, A., Kotlarski, S., Messeri, A., Morabito, M., Flouris, A. D., et al.
535 (2019). Overview of Existing Heat-Health Warning Systems in Europe. *International*
536 *Journal of Environmental Research and Public Health*, 16(15), 2657.
537 <https://doi.org/10.3390/ijerph16152657>
- 538 Crowhurst, D., Morrison, R., Evans, J., Cooper, H., Cumming, A., Fry, M., & Boorman, D.
539 (2019, September). *Actual evaporation data system for COSMOS-UK*. Workshop
540 presented at the Hydro-JULES: Next Generation Land Surface and Hydrological
541 Predictions, The Royal Society, London. Retrieved from
542 <http://nora.nerc.ac.uk/id/eprint/525105/>
- 543 Dirmeyer, P. A., Schlosser, C. A., & Brubaker, K. L. (2009). Precipitation, Recycling, and Land
544 Memory: An Integrated Analysis. *Journal of Hydrometeorology*, 10(1), 278–288.
545 <https://doi.org/10.1175/2008JHM1016.1>
- 546 Dirmeyer, P. A., Balsamo, G., & Peters-Lidard, C. D. (2015). Land-Atmosphere Interactions
547 and the Water Cycle. In *Seamless Prediction of the Earth System: from Minutes to Months*
548 *(G Brunet, S Jones, PM Ruti Eds.)* (pp. 145–154). Geneva, Switzerland: World
549 Meteorological Organization.
- 550 Dirmeyer, P. A., Gentine, P., Ek, M. B., & Balsamo, G. (2018). Land Surface Processes
551 Relevant to S2S Prediction. In *The Gap Between Weather and Climate Forecasting: Sub-*
552 *Seasonal to Seasonal Prediction* (Vol. A. W. Robertson and F. Vitart Eds., pp. 166–182).
553 Elsevier.

554 Dirmeyer, P. A., Chen, L., Wu, J., Shin, C.-S., Huang, B., Cash, B. A., et al. (2018). Verification
555 of Land–Atmosphere Coupling in Forecast Models, Reanalyses, and Land Surface
556 Models Using Flux Site Observations. *Journal of Hydrometeorology*, 19(2), 375–392.
557 <https://doi.org/10.1175/JHM-D-17-0152.1>

558 Ek, M. B., & Holtslag, A. a. M. (2004). Influence of Soil Moisture on Boundary Layer Cloud
559 Development. *Journal of Hydrometeorology*, 5(1), 86–99. [https://doi.org/10.1175/1525-
560 7541\(2004\)005<0086:IOSMOB>2.0.CO;2](https://doi.org/10.1175/1525-7541(2004)005<0086:IOSMOB>2.0.CO;2)

561 Evans, J. G., Ward, H. C., Blake, J. R., Hewitt, E. J., Morrison, R., Fry, M., et al. (2016). Soil
562 water content in southern England derived from a cosmic-ray soil moisture observing
563 system – COSMOS-UK. *Hydrological Processes*, 30(26), 4987–4999.
564 <https://doi.org/10.1002/hyp.10929>

565 Fischer, E. M., Seneviratne, S. I., Lüthi, D., & Schär, C. (2007). Contribution of land-
566 atmosphere coupling to recent European summer heat waves. *Geophysical Research
567 Letters*, 34(6). <https://doi.org/10.1029/2006GL029068>

568 Fratini, G., & Mauder, M. (2014). Towards a consistent eddy-covariance processing: an
569 intercomparison of EddyPro and TK3. *Atmospheric Measurement Techniques*, 7(7), 2273–
570 2281. <https://doi.org/10.5194/amt-7-2273-2014>

571 Gentine, P., Holtslag, A. A. M., D’Andrea, F., & Ek, M. (2013). Surface and Atmospheric
572 Controls on the Onset of Moist Convection over Land. *Journal of Hydrometeorology*,
573 14(5), 1443–1462. <https://doi.org/10.1175/JHM-D-12-0137.1>

574 Hersbach, H., Bell, B., Berrisford, P., Hirahara, S., Horányi, A., Muñoz-Sabater, J., et al.
575 (2020). The ERA5 Global Reanalysis. *Quarterly Journal of the Royal Meteorological
576 Society*, (accepted). <https://doi.org/10.1002/qj.3803>

577 Hirsch, A. L., Pitman, A. J., Seneviratne, S. I., Evans, J. P., & Haverd, V. (2014). Summertime
578 maximum and minimum temperature coupling asymmetry over Australia determined
579 using WRF. *Geophysical Research Letters*, 41(5), 1546–1552.
580 <https://doi.org/10.1002/2013GL059055>

581 Horst, S. V. J. van der, Pitman, A. J., Kauwe, M. G. D., Ukkola, A., Abramowitz, G., & Isaac,
582 P. (2019). How representative are FLUXNET measurements of surface fluxes during
583 temperature extremes? *Biogeosciences*, 16(8), 1829–1844. [https://doi.org/10.5194/bg-
584 16-1829-2019](https://doi.org/10.5194/bg-16-1829-2019)

585 Kendon, M., McCarthy, M., Jevrejeva, S., Matthews, A., & Legg, T. (2019). State of the UK
586 climate 2018. *International Journal of Climatology*, 39(S1), 1–55.
587 <https://doi.org/10.1002/joc.6213>

588 Kornhuber, K., Osprey, S., Coumou, D., Petri, S., Petoukhov, V., Rahmstorf, S., & Gray, L.
589 (2019). Extreme weather events in early summer 2018 connected by a recurrent
590 hemispheric wave-7 pattern. *Environmental Research Letters*, 14(5), 054002.
591 <https://doi.org/10.1088/1748-9326/ab13bf>

592 Koster, R. D., Sud, Y. C., Guo, Z., Dirmeyer, P. A., Bonan, G., Oleson, K. W., et al. (2006).
593 GLACE: The Global Land–Atmosphere Coupling Experiment. Part I: Overview. *Journal of
594 Hydrometeorology*, 7(4), 590–610. <https://doi.org/10.1175/JHM510.1>

595 Lass, W., Haas, A., Hinkel, J., & Jaeger, C. (2011). Avoiding the avoidable: Towards a
596 European heat waves risk governance. *International Journal of Disaster Risk Science*, 2(1),
597 1–14. <https://doi.org/10.1007/s13753-011-0001-z>

598 Lau, N.-C., & Nath, M. J. (2014). Model Simulation and Projection of European Heat Waves
599 in Present-Day and Future Climates. *Journal of Climate*, 27(10), 3713–3730.
600 <https://doi.org/10.1175/JCLI-D-13-00284.1>

601 Magnusson, L., Ferranti, L., & Vamborg, F. (2018). Forecasting the 2018 European
602 heatwave. *ECMWF Newsletter*, 157, 2–3.

603 Miralles, D. G., Gentine, P., Seneviratne, S. I., & Teuling, A. J. (2018). Land–atmospheric
604 feedbacks during droughts and heatwaves: state of the science and current challenges.
605 *Annals of the New York Academy of Sciences*, 0(0), 1–17.
606 <https://doi.org/10.1111/nyas.13912>

607 Morrison, R., Cooper, H., Cumming, A., Scarlett, P., Thornton, J., & Winterbourn, B. (2019).
608 Eddy covariance measurements of carbon dioxide, energy and water fluxes at an
609 organically managed grassland, Berkshire, UK, 2017 to 2019. Retrieved May 18, 2020,
610 from <https://catalogue.ceh.ac.uk/id/5a93161f-0124-4650-a2c9-7e8aaea7e6bb>

611 Morrison, R., Cooper, H., Cumming, A., Evans, C., Thomson, J., Winterbourn, B., et al.
612 (2020). Eddy covariance measurements of carbon dioxide, energy and water fluxes at a
613 cropland and a grassland on lowland peat soils, East Anglia, UK, 2016–2019. Retrieved
614 May 18, 2020, from <https://catalogue.ceh.ac.uk/id/2fe84b80-117a-4b19-a1f5-71bbd1db9c9>

616 Muggeo, V. M., & Hajat, S. (2009). Modelling the non-linear multiple-lag effects of ambient
617 temperature on mortality in Santiago and Palermo: a constrained segmented distributed
618 lag approach. *Occupational and Environmental Medicine*, 66(9), 584–591.
619 <https://doi.org/10.1136/oem.2007.038653>

620 Muggeo, V. M. R. (2003). Estimating regression models with unknown break-points.
621 *Statistics in Medicine*, 22(19), 3055–3071. <https://doi.org/10.1002/sim.1545>

622 Nogueira, M., Albergel, C., Boussetta, S., Johannsen, F., Trigo, I. F., Ermida, S. L., et al.
623 (2020). Role of vegetation in representing land surface temperature in the CHTESSEL
624 (CY45R1) and SURFEX-ISBA (v8.1) land surface models: a case study over Iberia.
625 *Geoscientific Model Development Discussions*, 1–29. [https://doi.org/10.5194/gmd-2020-](https://doi.org/10.5194/gmd-2020-49)
626 49

627 Papale, D., Reichstein, M., Aubinet, M., Canfora, E., Bernhofer, C., Kutsch, W., et al. (2006).
628 Towards a standardized processing of Net Ecosystem Exchange measured with eddy
629 covariance technique: algorithms and uncertainty estimation. *Biogeosciences*, 3(4), 571–
630 583. <https://doi.org/10.5194/bg-3-571-2006>

631 Petch, J. C., Short, C. J., Best, M. J., McCarthy, M., Lewis, H. W., Vosper, S. B., & Weeks, M.
632 (2020). Sensitivity of the 2018 UK summer heatwave to local sea temperatures and soil
633 moisture. *Atmospheric Science Letters*, 21(3), e948. <https://doi.org/10.1002/asl.948>

634 Philip, S. Y., Kew, S. F., Hauser, M., Guillod, B. P., Teuling, A. J., Whan, K., et al. (2018).
635 Western US high June 2015 temperatures and their relation to global warming and soil
636 moisture. *Climate Dynamics*, 50(7–8), 2587–2601. [https://doi.org/10.1007/s00382-017-](https://doi.org/10.1007/s00382-017-3759-x)
637 3759-x

638 Reichstein, M., Falge, E., Baldocchi, D., Papale, D., Aubinet, M., Berbigier, P., et al. (2005).
639 On the separation of net ecosystem exchange into assimilation and ecosystem
640 respiration: review and improved algorithm. *Global Change Biology*, 11(9), 1424–1439.
641 <https://doi.org/10.1111/j.1365-2486.2005.001002.x>

642 de Rosnay, P., Balsamo, G., Albergel, C., Muñoz-Sabater, J., & Isaksen, L. (2014).
643 Initialisation of Land Surface Variables for Numerical Weather Prediction. *Surveys in*
644 *Geophysics*, 35(3), 607–621. <https://doi.org/10.1007/s10712-012-9207-x>
645 Rösner, B., Benedict, I., van Heerwaarden, C., Weerts, A., Hazeleger, W., Bissolli, P., &
646 Trachte, K. (2019). The long heat wave and drought in Europe in 2018. *Bulletin of the*
647 *American Meteorological Society*, 100(9), S222–S223.
648 <https://doi.org/10.1175/2019BAMSStateoftheClimate.1>
649 Rosolem, R., Shuttleworth, W. J., Zreda, M., Franz, T. E., Zeng, X., & Kurc, S. A. (2013). The
650 Effect of Atmospheric Water Vapor on Neutron Count in the Cosmic-Ray Soil Moisture
651 Observing System. *Journal of Hydrometeorology*, 14(5), 1659–1671.
652 <https://doi.org/10.1175/JHM-D-12-0120.1>
653 Russo, S., Sillmann, J., & Fischer, E. M. (2015). Top ten European heatwaves since 1950 and
654 their occurrence in the coming decades. *Environmental Research Letters*, 10(12), 124003.
655 <https://doi.org/10.1088/1748-9326/10/12/124003>
656 Samaniego, L., Thober, S., Kumar, R., Wanders, N., Rakovec, O., Pan, M., et al. (2018).
657 Anthropogenic warming exacerbates European soil moisture droughts. *Nature Climate*
658 *Change*, 8(5), 421–426. <https://doi.org/10.1038/s41558-018-0138-5>
659 Santanello, J. A., Friedl, M. A., & Ek, M. B. (2007). Convective Planetary Boundary Layer
660 Interactions with the Land Surface at Diurnal Time Scales: Diagnostics and Feedbacks.
661 *Journal of Hydrometeorology*, 8(5), 1082–1097. <https://doi.org/10.1175/JHM614.1>
662 Santanello, J. A., Peters-Lidard, C. D., Kumar, S. V., Alonge, C., & Tao, W.-K. (2009). A
663 Modeling and Observational Framework for Diagnosing Local Land–Atmosphere
664 Coupling on Diurnal Time Scales. *Journal of Hydrometeorology*, 10(3), 577–599.
665 <https://doi.org/10.1175/2009JHM1066.1>
666 Santanello, J. A., Peters-Lidard, C. D., & Kumar, S. V. (2011). Diagnosing the Sensitivity of
667 Local Land–Atmosphere Coupling via the Soil Moisture–Boundary Layer Interaction.
668 *Journal of Hydrometeorology*, 12(5), 766–786. <https://doi.org/10.1175/JHM-D-10-05014.1>
669 Santanello, J. A., Dirmeyer, P. A., Ferguson, C. R., Findell, K. L., Tawfik, A. B., Berg, A., et al.
670 (2018). Land-Atmosphere Interactions: The LoCo Perspective. *Bulletin of the American*
671 *Meteorological Society*, 99, 1253–1272. <https://doi.org/10.1175/BAMS-D-17-0001.1>
672 Schumacher, D. L., Keune, J., Heerwaarden, C. C. van, Arellano, J. V.-G. de, Teuling, A. J., &
673 Miralles, D. G. (2019). Amplification of mega-heatwaves through heat torrents fuelled by
674 upwind drought. *Nature Geoscience*, 12(9), 712–717. [https://doi.org/10.1038/s41561-019-](https://doi.org/10.1038/s41561-019-0431-6)
675 [0431-6](https://doi.org/10.1038/s41561-019-0431-6)
676 Schwingshackl, C., Hirschi, M., & Seneviratne, S. I. (2018). A theoretical approach to assess
677 soil moisture–climate coupling across CMIP5 and GLACE-CMIP5 experiments. *Earth*
678 *System Dynamics*, 9(4), 1217–1234. <https://doi.org/10.5194/esd-9-1217-2018>
679 Seneviratne, S. I., Lüthi, D., Litschi, M., & Schär, C. (2006). Land–atmosphere coupling and
680 climate change in Europe. *Nature*, 443(7108), 205–209.
681 <https://doi.org/10.1038/nature05095>
682 Seneviratne, S. I., Corti, T., Davin, E. L., Hirschi, M., Jaeger, E. B., Lehner, I., et al. (2010).
683 Investigating soil moisture–climate interactions in a changing climate: A review. *Earth-*
684 *Science Reviews*, 99(3), 125–161. <https://doi.org/10.1016/j.earscirev.2010.02.004>

685 Sousa, P. M., Barriopedro, D., Ramos, A. M., García-Herrera, R., Espírito-Santo, F., & Trigo,
686 R. M. (2019). Saharan air intrusions as a relevant mechanism for Iberian heatwaves: The
687 record breaking events of August 2018 and June 2019. *Weather and Climate Extremes*,
688 26, 100224. <https://doi.org/10.1016/j.wace.2019.100224>

689 Stanley, S., Antoniou, V., Ball, L. A., Bennett, E. S., Blake, J. R., Boorman, D. B., et al. (2019).
690 Daily and sub-daily hydrometeorological and soil data (2013-2017) [COSMOS-UK].
691 Retrieved May 18, 2020, from [https://catalogue.ceh.ac.uk/id/a6012796-291c-4fd6-a7ef-
692 6f6ed0a6cfa5](https://catalogue.ceh.ac.uk/id/a6012796-291c-4fd6-a7ef-6f6ed0a6cfa5)

693 Teuling, A. J. (2018). A hot future for European droughts. *Nature Climate Change*, 8(5), 364–
694 365. <https://doi.org/10.1038/s41558-018-0154-5>

695 Vicente-Serrano, S. M., Lopez-Moreno, J.-I., Beguería, S., Lorenzo-Lacruz, J., Sanchez-
696 Lorenzo, A., García-Ruiz, J. M., et al. (2014). Evidence of increasing drought severity
697 caused by temperature rise in southern Europe. *Environmental Research Letters*, 9(4),
698 044001. <https://doi.org/10.1088/1748-9326/9/4/044001>

699 Wolf, S., Keenan, T. F., Fisher, J. B., Baldocchi, D. D., Desai, A. R., Richardson, A. D., et al.
700 (2016). Warm spring reduced carbon cycle impact of the 2012 US summer drought.
701 *Proceedings of the National Academy of Sciences*, 113(21), 5880–5885.
702 <https://doi.org/10.1073/pnas.1519620113>

703 Wu, J., & Dirmeyer, P. A. (2020). Drought Demise Attribution Over CONUS. *Journal of*
704 *Geophysical Research: Atmospheres*, 125(4), e2019JD031255.
705 <https://doi.org/10.1029/2019JD031255>

706 Zhang, Y., Wang, L., Santanello, J. A., Pan, Z., Gao, Z., & Li, D. (2020). Aircraft observed
707 diurnal variations of the planetary boundary layer under heat waves. *Atmospheric*
708 *Research*, 235, 104801. <https://doi.org/10.1016/j.atmosres.2019.104801>

709 Zscheischler, J., Westra, S., Hurk, B. J. J. M. van den, Seneviratne, S. I., Ward, P. J., Pitman,
710 A., et al. (2018). Future climate risk from compound events. *Nature Climate Change*, 8(6),
711 469–477. <https://doi.org/10.1038/s41558-018-0156-3>

712

713

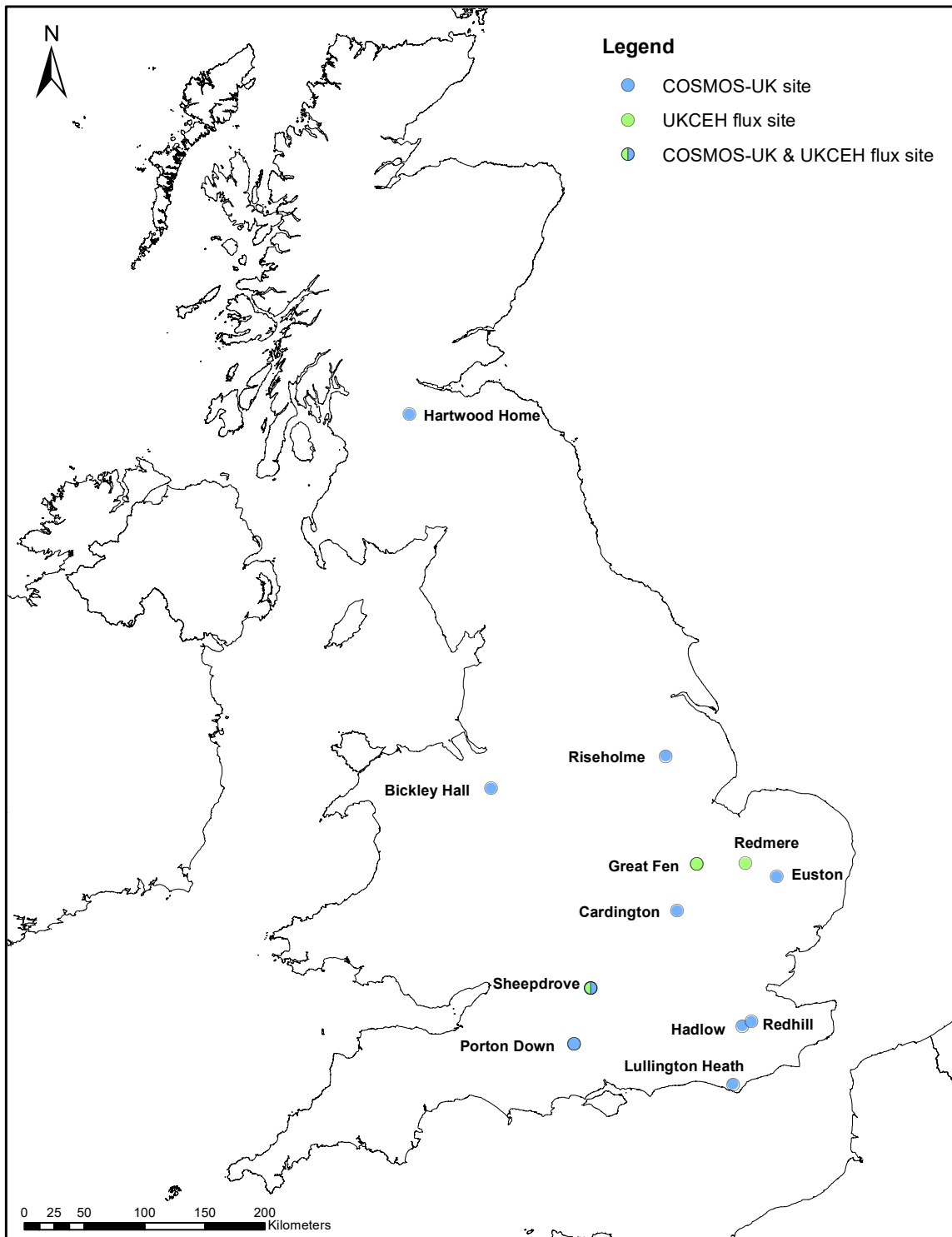
714 **Table 1.** Mean difference and root mean square difference (RMSE) between volumetric soil
 715 moisture content values at breakpoint when estimated using daily maximum temperature (as in
 716 Figure 6) versus the indicated surface flux terms (EF = evaporative fraction, SH = sensible heat
 717 flux, LH = latent heat flux). The domain for calculations is as in Figure 6, units are m^3m^{-3} .

718

	Mean Difference			RMSE		
	EF	SH	LH	EF	SH	LH
May	0.008	0.001	0.028	0.061	0.049	0.063
June	0.007	-0.006	0.028	0.053	0.049	0.064
July	-0.003	0.011	0.041	0.054	0.048	0.074
August	-0.007	0.005	0.028	0.054	0.050	0.067

719

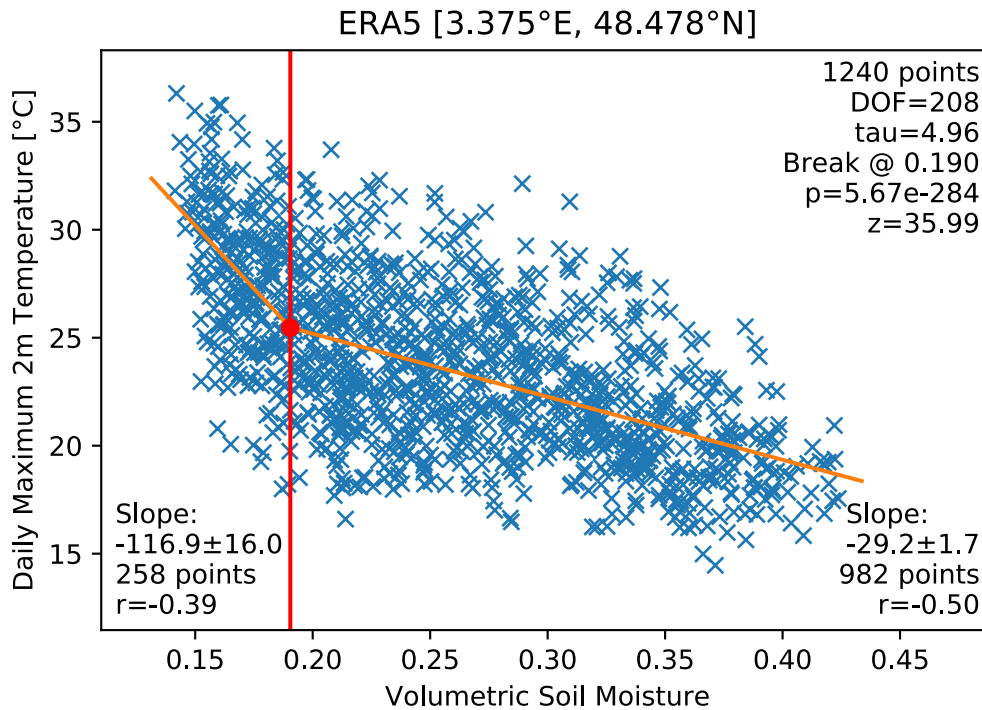
720



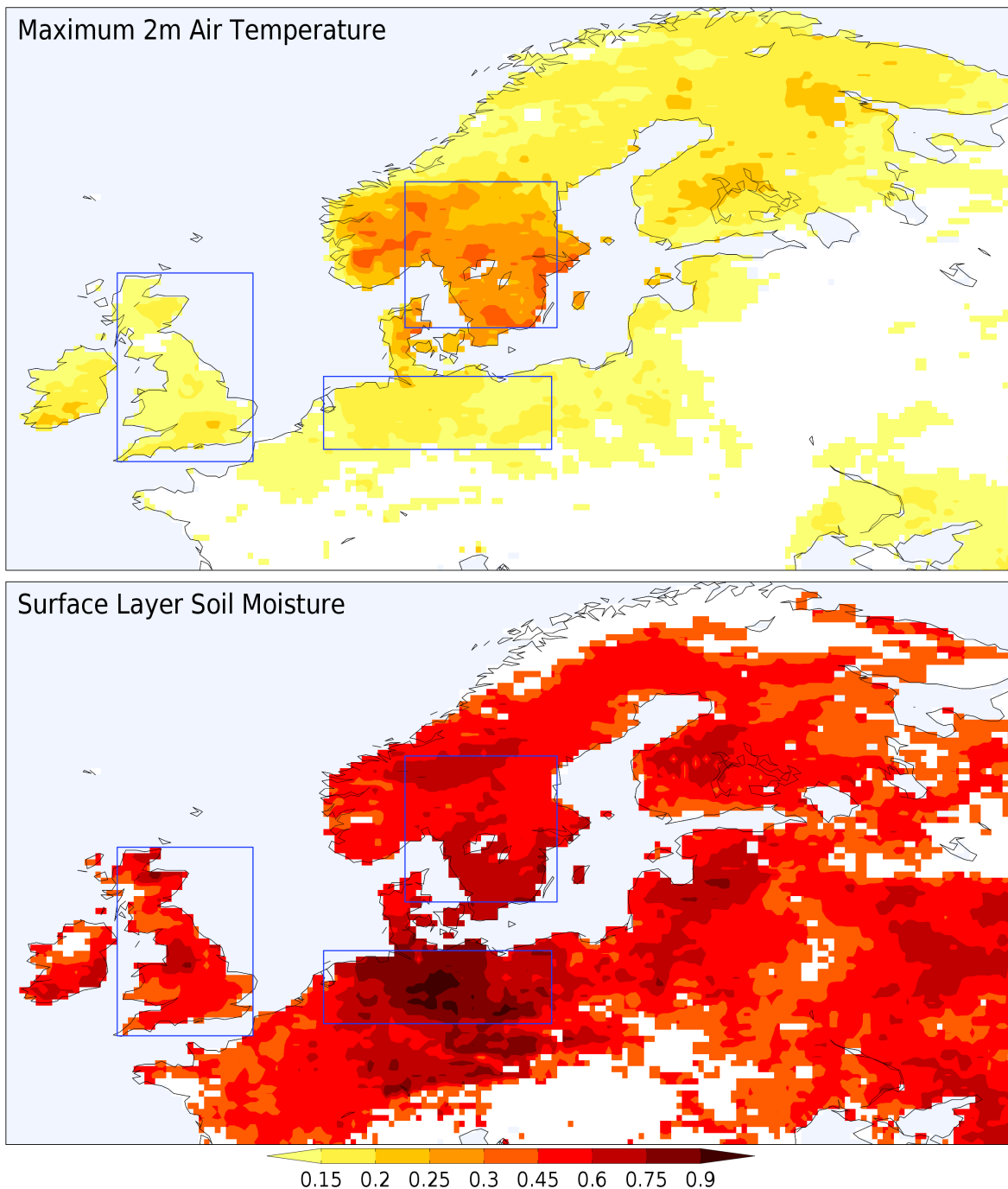
721 **Figure 1.** Locations of soil moisture and flux tower sites in Britain used in this study.

722

723

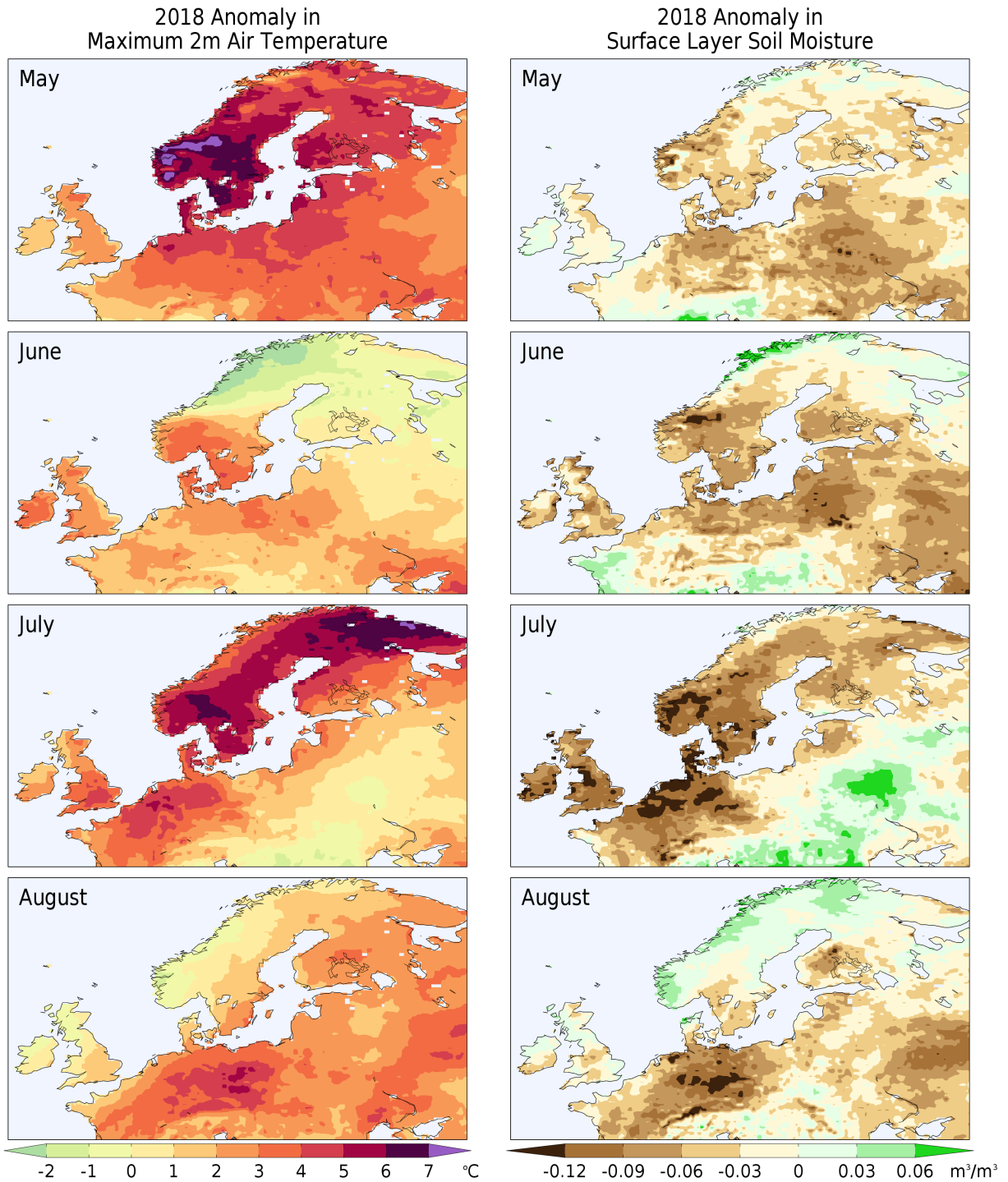


724 **Figure 2:** Relationship between daily maximum 2m air temperature (dependent variable;
 725 ordinate) and surface volumetric soil moisture (abscissa) during July for 1979-2018 at a grid cell
 726 in France. Values in upper right refer to the total number of days (including soil moisture memory
 727 time scale “tau” in days and reduced degrees of freedom “DOF” due to soil moisture
 728 autocorrelation) and significance of the estimate of the breakpoint between two best-fit linear
 729 regressions. Values in the lower corners show the estimated slopes, standard error of estimates,
 730 number of points and correlations for each segment – the fits for each segment are significant at
 731 the 99% confidence level.

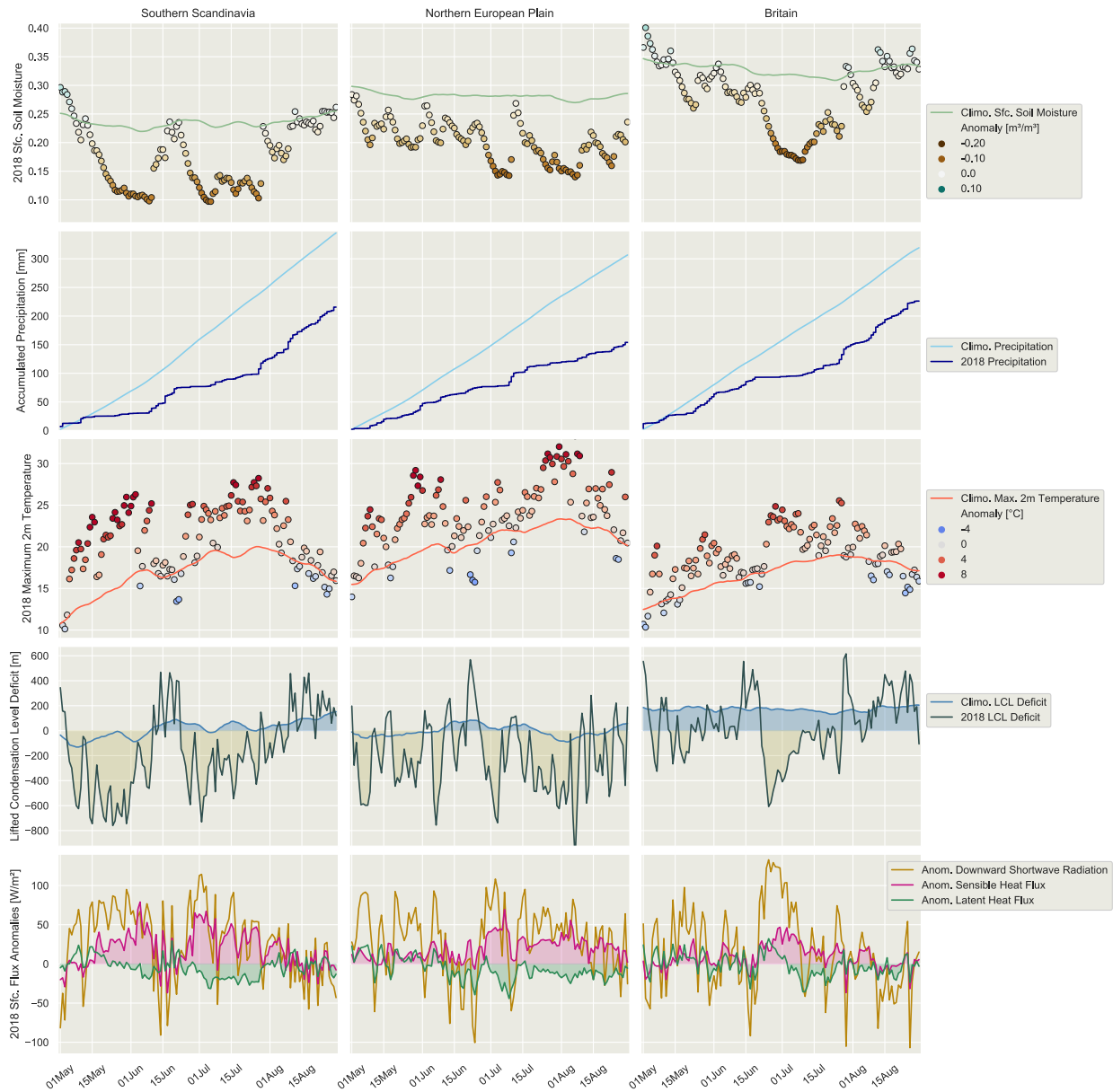


732 **Figure 3:** Fraction of days during May, June, July and August 2018 that are among 5% of warmest
 733 anomalies in maximum 2m air temperature (top); 25% driest absolute surface layer volumetric
 734 soil water content (bottom); compared to all days in May, June, July and August of 1979-2018.
 735 Colored areas are significant at the 99% confidence level. Blue boxes outline regions where land-
 736 only averages are shown in Figure 5.

737
 738

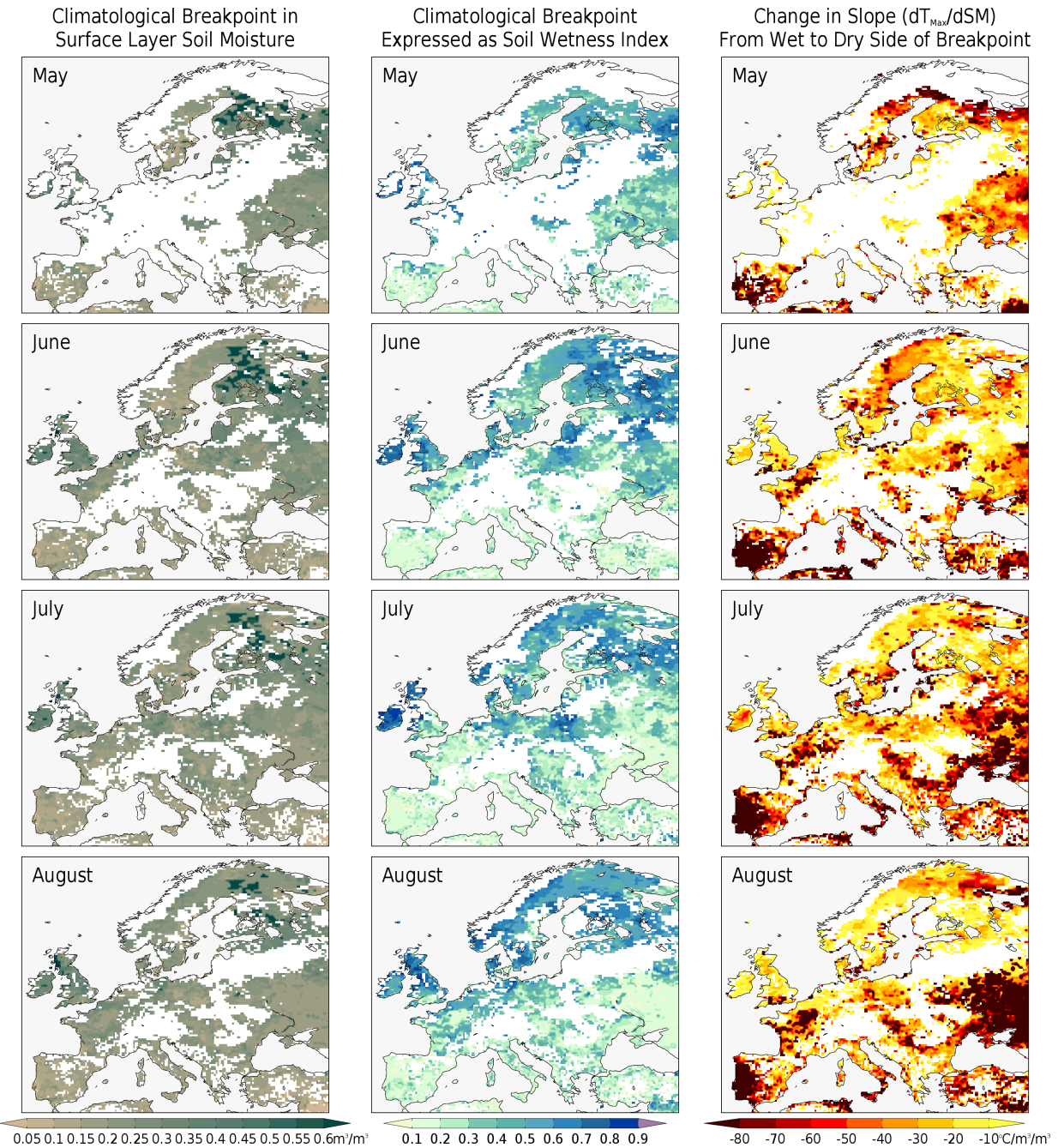


739 **Figure 4:** Monthly anomalies during 2018 in daily maximum 2m air temperature (left column) and
 740 surface volumetric soil water content (right column) in ERA5 compared to the 1979-2018 mean.
 741

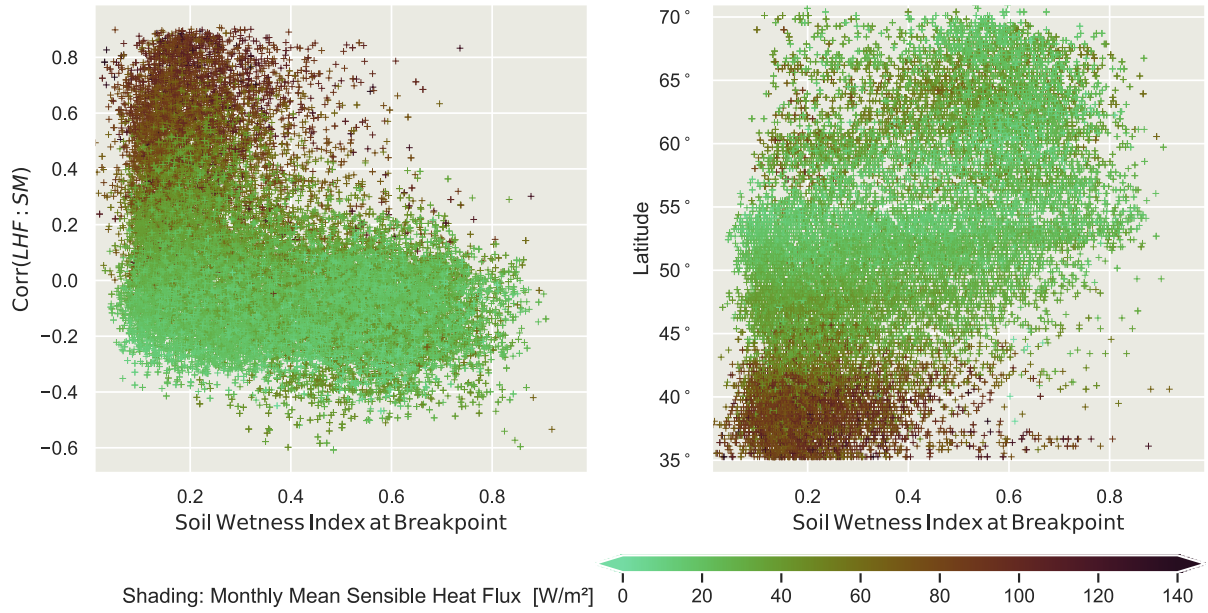


742 **Figure 5:** Area averages from ERA5 over the regions indicated in Figure 3 of daily surface layer
 743 volumetric soil water content (top row), cumulative precipitation (second row), daily maximum
 744 2m air temperature (third row), LCL deficit (fourth row) and indicated surface energy balance
 745 terms (bottom row). In each panel, climatological values are indicated by a smooth (7-day
 746 centered running mean) line except in the bottom row where only anomalies are shown. In the
 747 first and third rows, color of dots indicates the magnitude of the anomaly.

748
 749

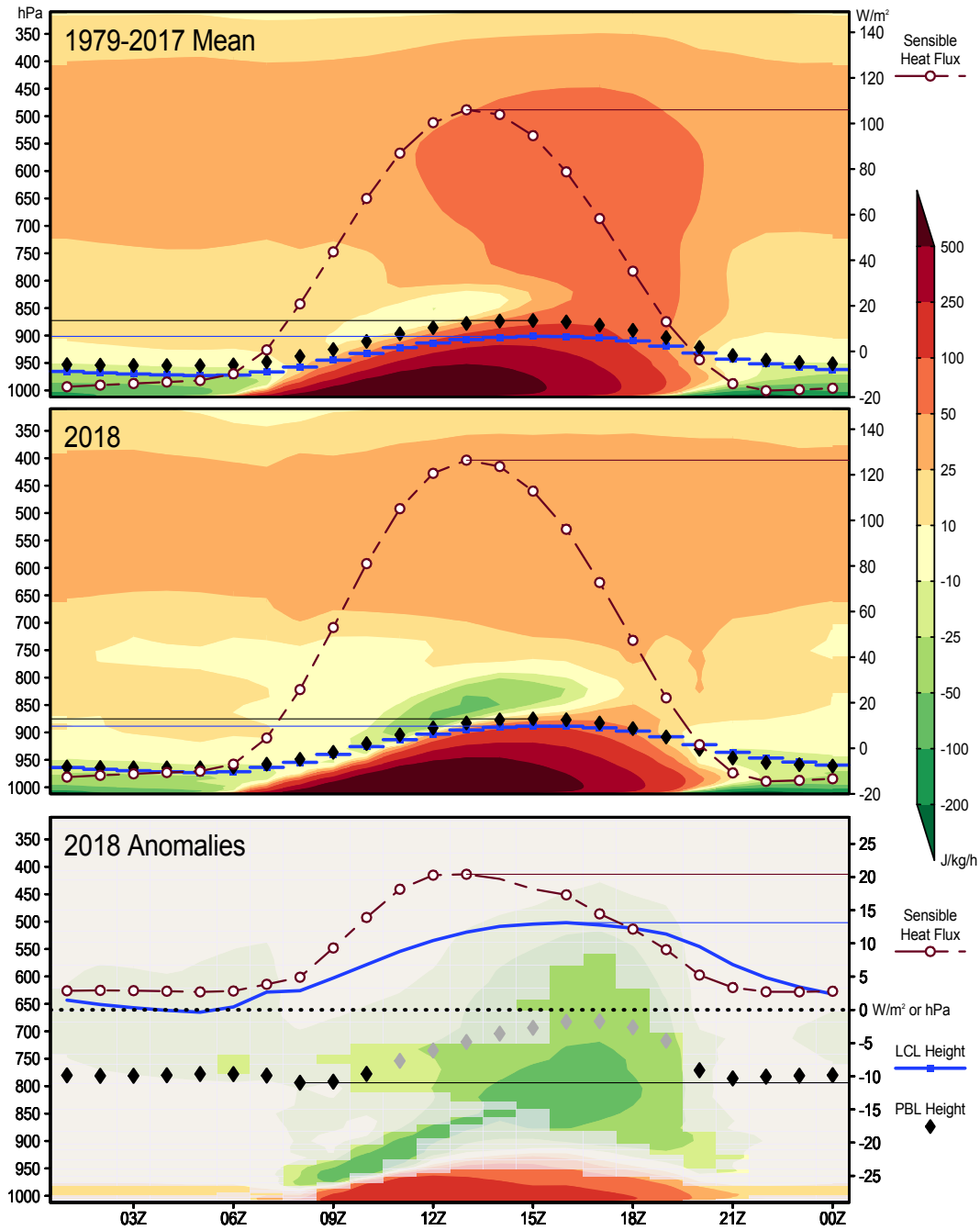


750 **Figure 6:** Values of volumetric soil water content (left column) and soil wetness index (middle
 751 column; see text for description) estimated to be at the breakpoint regarding a change in the
 752 slope of the regression of daily maximum 2m air temperature on soil water content. The right
 753 column shows the change in the slope of the regression. White areas fail to pass at least one of
 754 the criteria described in Section 3, with an additional criterion that the estimated value of the
 755 maximum temperature at the breakpoint exceed 10°C.
 756

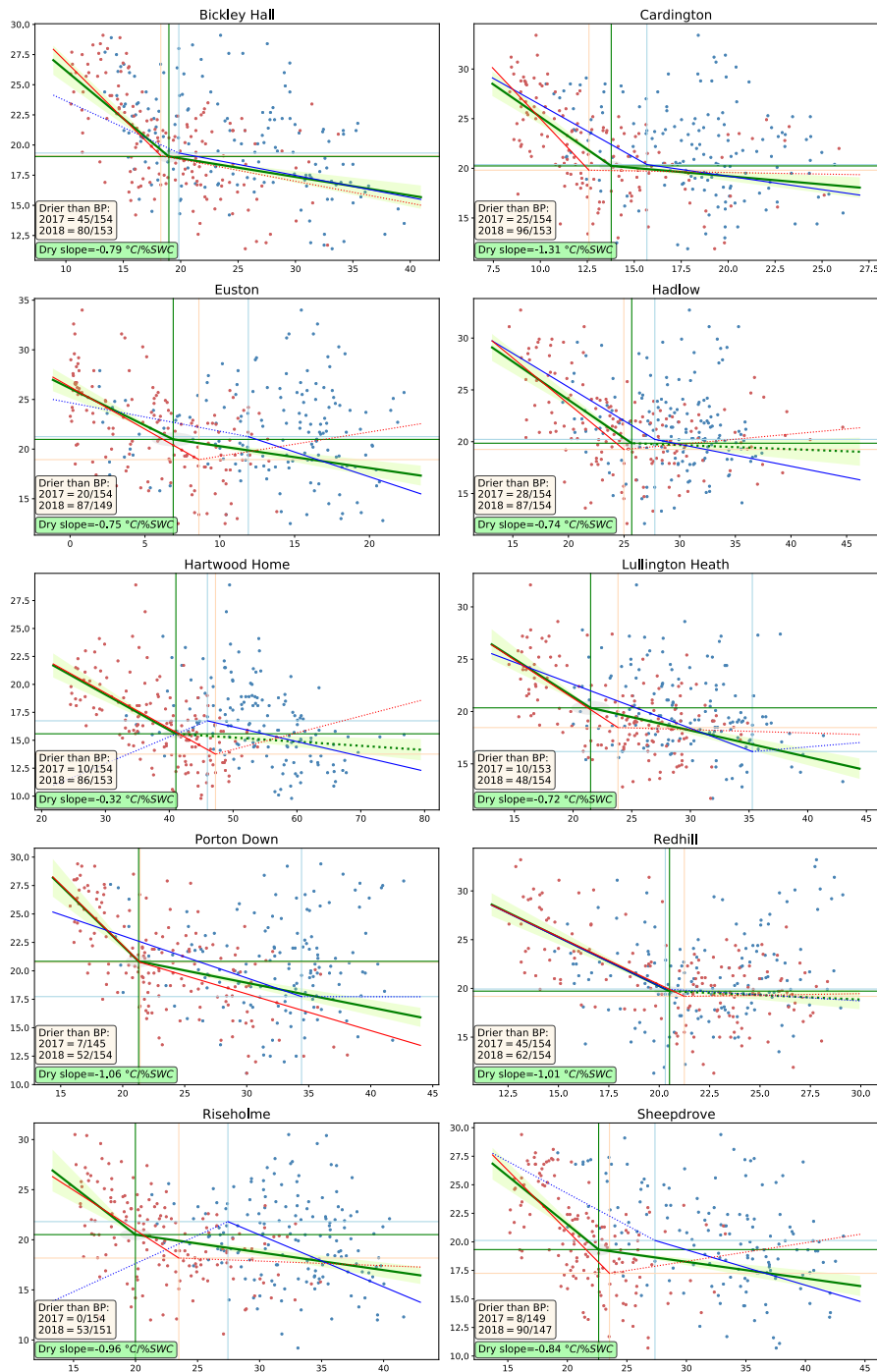


757 **Figure 7:** Scatter plots relating the estimated monthly breakpoint values of soil wetness index
 758 estimated for May, June, July and August to the temporal correlation between latent heat flux
 759 and soil moisture (left panel), latitude (right panel) and surface sensible heat flux (color in both
 760 panels) using ERA5 data. Each point is one land grid cell and one of the four months over the
 761 European domain shown in Figure 6; estimates use 40 years of data (1979-2018).
 762

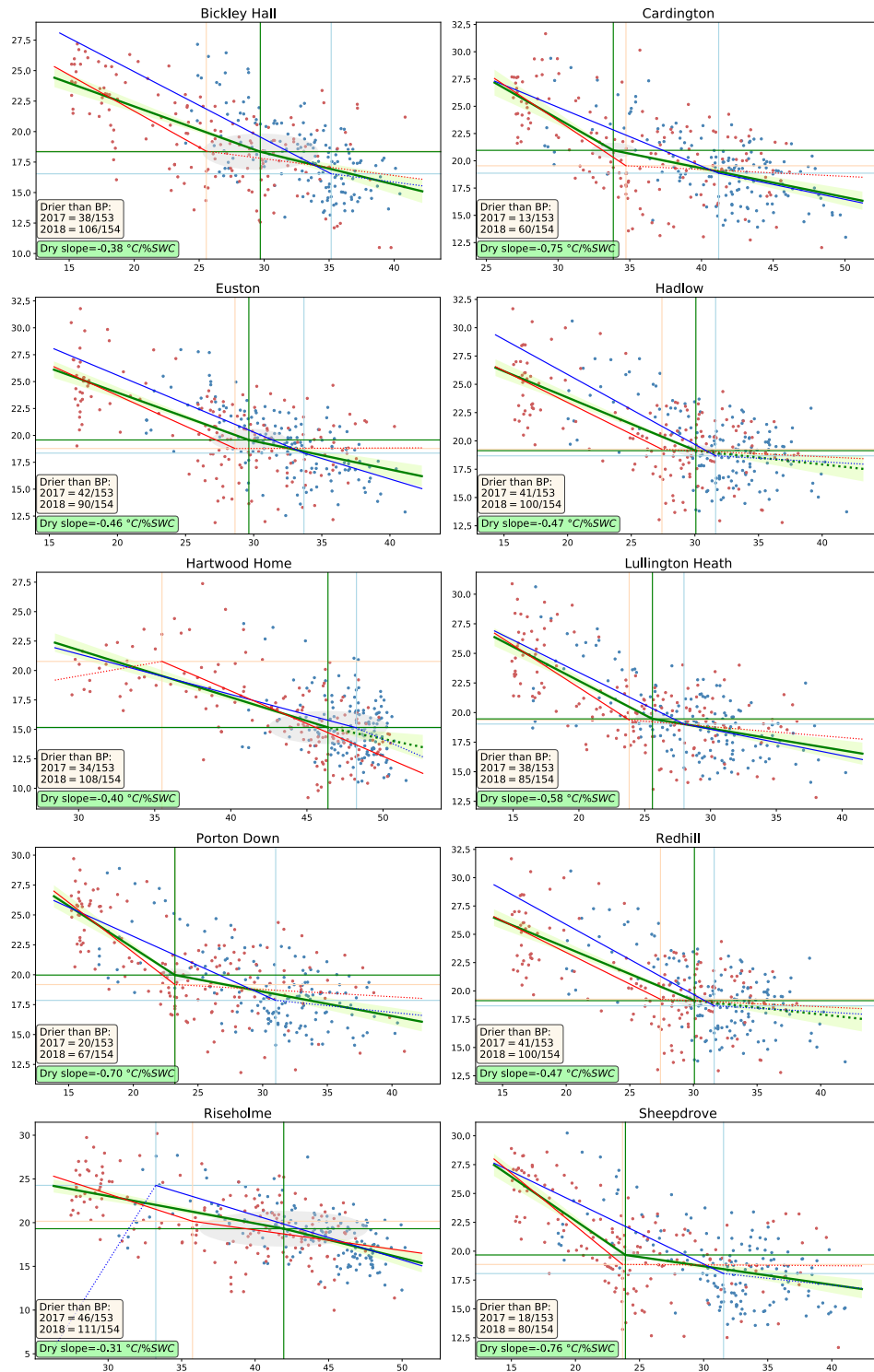
MJJA 2018 Britain (vs. 1979-2017 Mean)



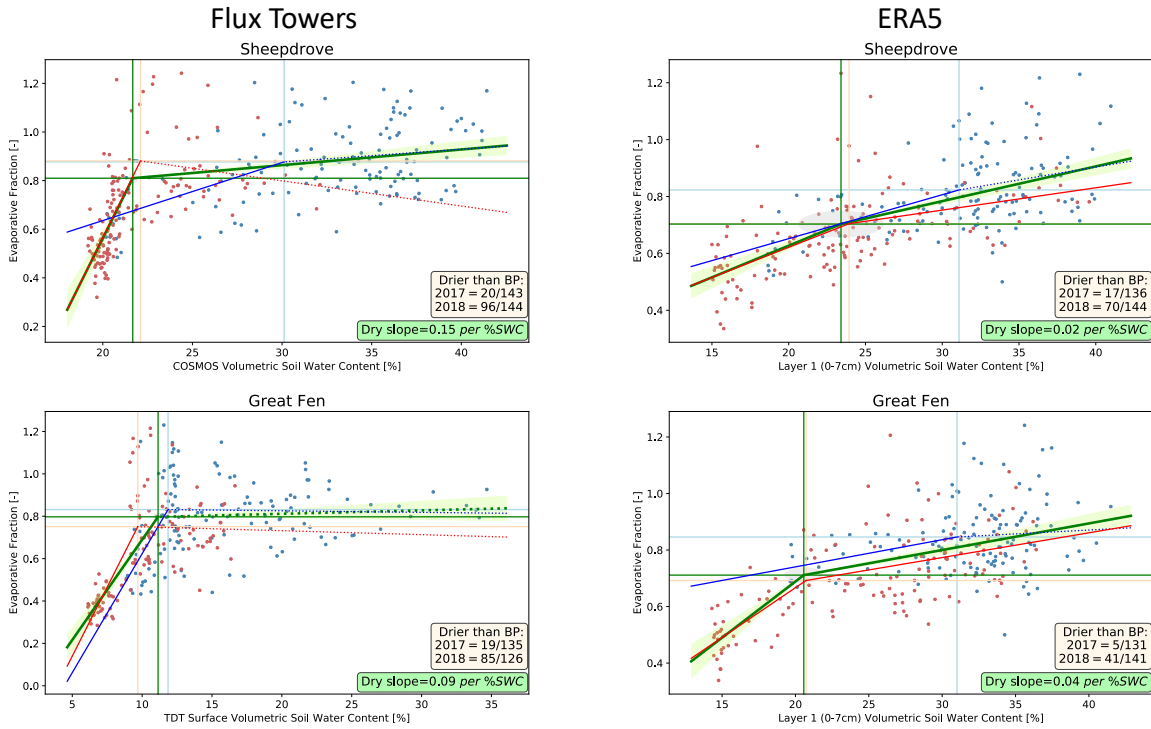
763 **Figure 8:** Time – height (model pseudo-pressure coordinate, scale on the left; see Section 2 for
 764 details) diagram of hourly heat budget terms averaged over land grid cells of Britain (see box in
 765 Figure 3) from ERA5 data. Shading is total diabatic heating per hour – insignificant anomalies for
 766 2018 are greyed out in the bottom panel. Lines and/or symbols show surface sensible heat flux,
 767 LCL height and PBL height as indicated, and thin horizontal lines mark daily extremes tailing to
 768 the appropriate scale. In the bottom panel, faint or missing hourly markers indicate lack of
 769 significance of the anomaly. All significances are at 95% confidence levels.
 770



771 **Figure 9:** Relationship between daily maximum 2m air temperature (dependent variable;
772 ordinate) and surface volumetric soil water content (abscissa) during 15 May through 15 October
773 for 2017 (blue) and 2018 (red) at indicated COSMOS-UK stations. Breakpoint analysis is
774 performed for each year, and the two years combined (green) where the light shading indicates
775 standard error in the estimate of the slopes. Dotted lines denote slopes that are below the 95%
776 confidence level. A grey ellipse centered on the 2-year breakpoint shows the range of standard
777 error along both axes. Values in the colored boxes show the regression slope (green) and the
778 number of points in each year (tan) on the dry side of the breakpoint.
779



780 **Figure 10:** As in Figure 9 for daily ERA5 grid cell data.
 781



782

783

784

785

Figure 11: As in Figures 9-10 for breakpoints of evaporative fraction as the dependent variable at flux tower field sites (left column) and ERA5 grid cells encompassing the sites (right column).

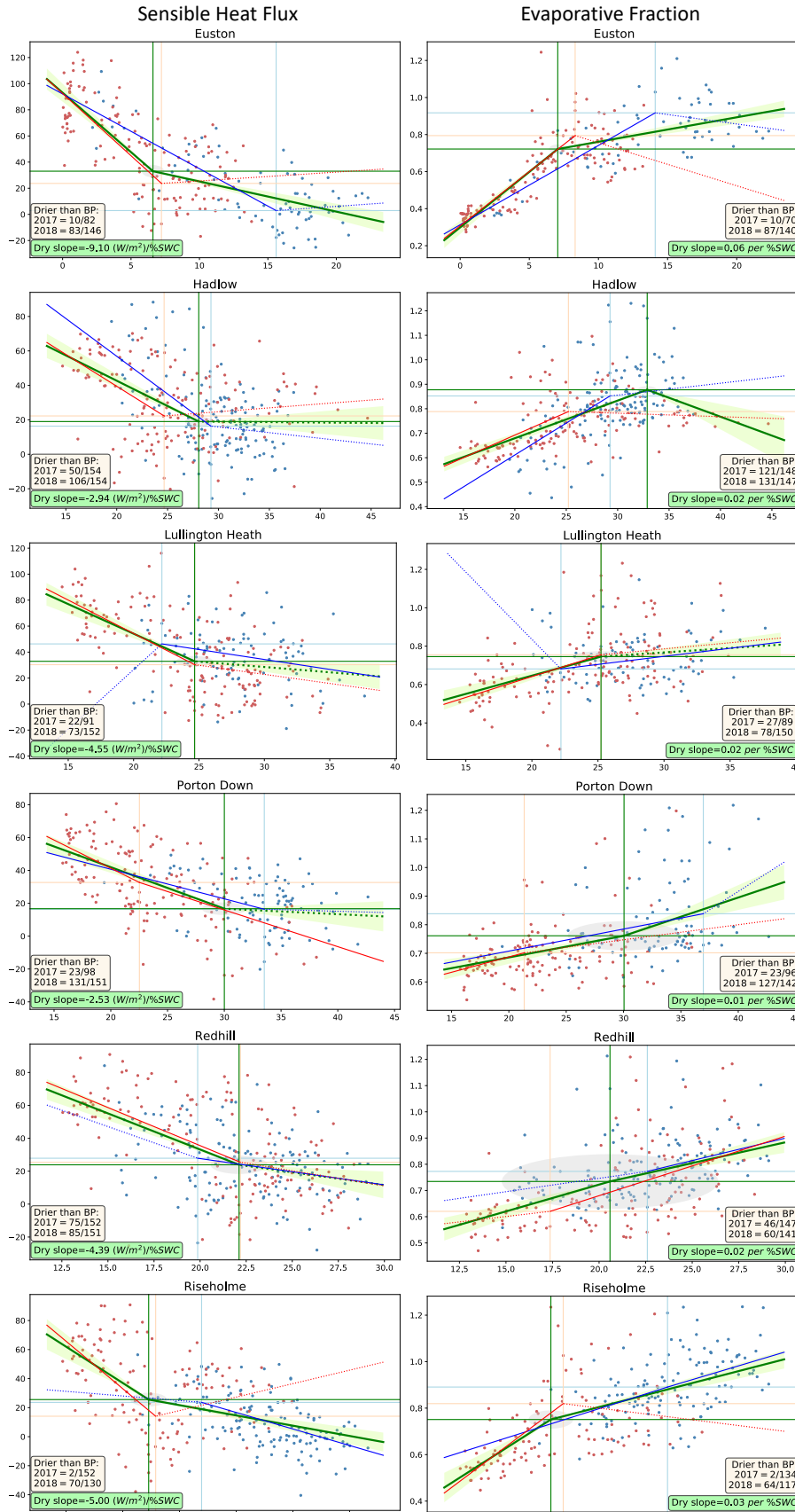
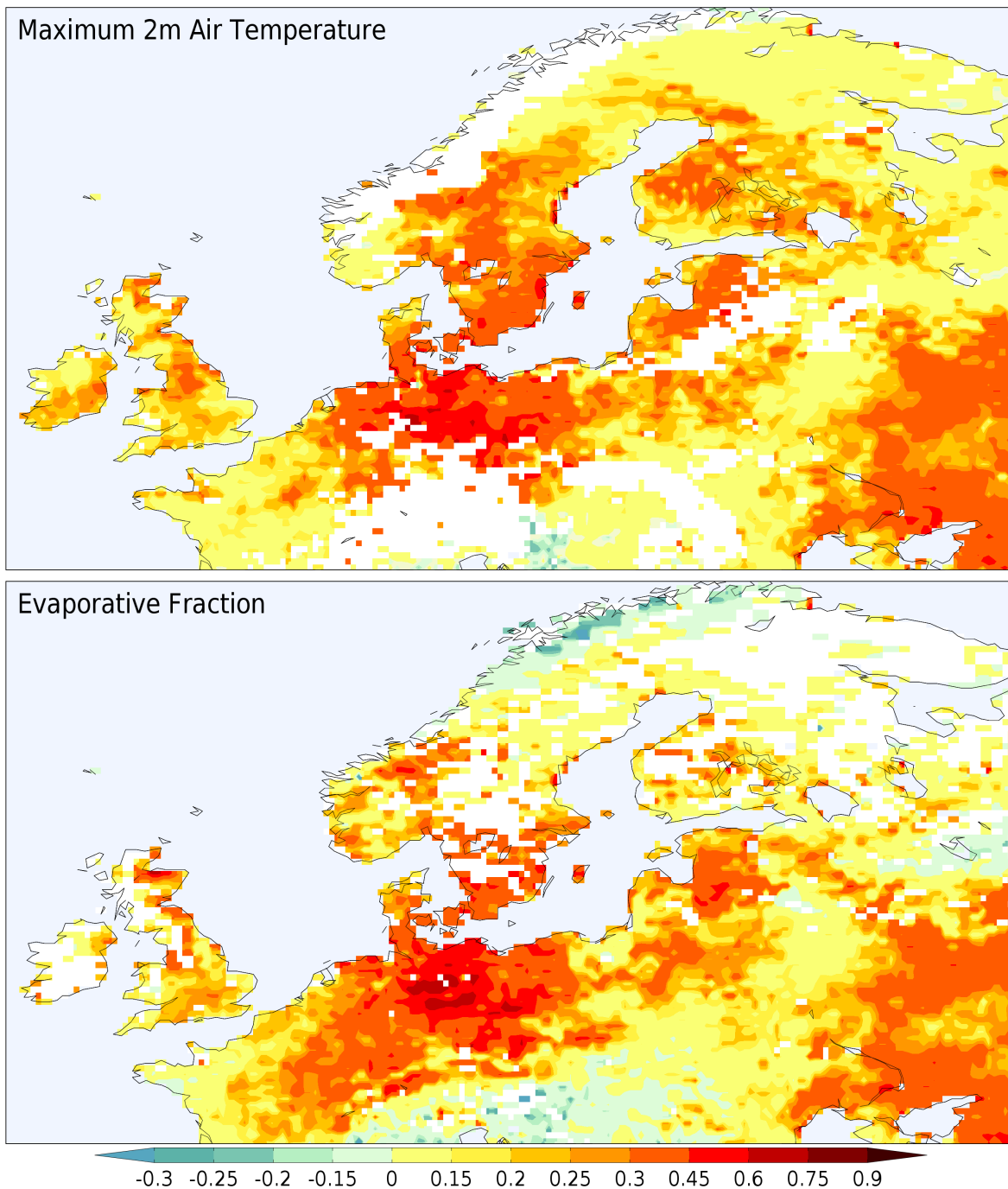


Figure 12: As in Figure 11 for COSMOS-UK sites with estimated surface heat fluxes: sensible heat in the left column (ordinate) and evaporative fraction in the right column (ordinate) versus surface volumetric soil water content (abscissa in both columns).



799
 800 **Figure 13:** Increase in the fraction of days during May-August on the dry side of the surface
 801 volumetric soil water content breakpoint based on ERA5 daily maximum temperature (top) and
 802 evaporative fraction (bottom) compared to the 1979-2018 average. Masked areas fail to meet
 803 the screening criteria described in Section 3 in all four months.

Supplemental material for:

Land-Atmosphere Interactions May Have Exacerbated the Drought and Heatwave over Northern Europe during Summer 2018

Paul A. Dirmeyer

Center for Ocean-Land-Atmosphere Studies, George Mason University, Fairfax, Virginia, USA

Gianpaolo Balsamo

European Centre for Medium-range Weather Forecasts, Reading, United Kingdom

Eleanor M. Blyth, Ross Morrison, and Hollie M. Cooper

UK Centre for Ecology and Hydrology, Wallingford, United Kingdom

Contents:

Tables S1-S2.

Figures S1-S8.

Table S1: Correlations between COSMOS stations and their encompassing ERA5 grid cells for daily time series of volumetric soil water content (VWC) and daily maximum temperature (T_{Max}). For each year, the period 15 May through 15 October is included in the calculation; days with missing data are excluded (of 154 days, the largest number missing is 10 for VWC, 7 for T_{Max}).

COSMOS Station	VWC 2017	VWC 2018	T_{Max} 2017	T_{Max} 2018
Bickley Hall	0.76	0.91	0.94	0.97
Cardington	0.83	0.66	0.94	0.97
Euston	0.73	0.86	0.95	0.97
Hadlow	0.78	0.68	0.96	0.97
Hartwood Home	0.69	0.85	0.93	0.95
Lullington Heath	0.78	0.89	0.93	0.93
Porton Down	0.81	0.89	0.95	0.96
Redhill	0.72	0.91	0.95	0.96
Riseholme	0.84	0.56	0.95	0.97
Sheepdrove	0.76	0.87	0.96	0.96

Table S2: Correlations between UKCEH flux towers and their encompassing ERA5 grid cells for daily time series of volumetric soil water content (VWC), latent heat flux (LHF), sensible heat flux (SHF), evaporative fraction (EF; values excluded if not in range $-0.1 \leq EF \leq 1.25$), net radiation (R_{Net}), 2m air temperature (T_{2m}), and precipitation (Prec). For each year, the period 15 May through 15 October is included in the calculation; days with missing data are excluded (7-18% missing for EF, otherwise 0-2% missing except 11% for 2018 VWC at Great Fen).

Flux Tower	Year	VWC	LHF	SHF	EF	R_{Net}	T_{2m}	Prec.
Sheepdrove	2017	0.78	0.84	0.77	0.69	0.88	0.99	0.89
	2018	0.70	0.68	0.86	0.68	0.90	0.99	0.78
Great Fen	2017	0.52	0.80	0.73	0.54	0.87	0.98	0.67
	2018	0.65	0.78	0.84	0.74	0.93	0.98	0.77

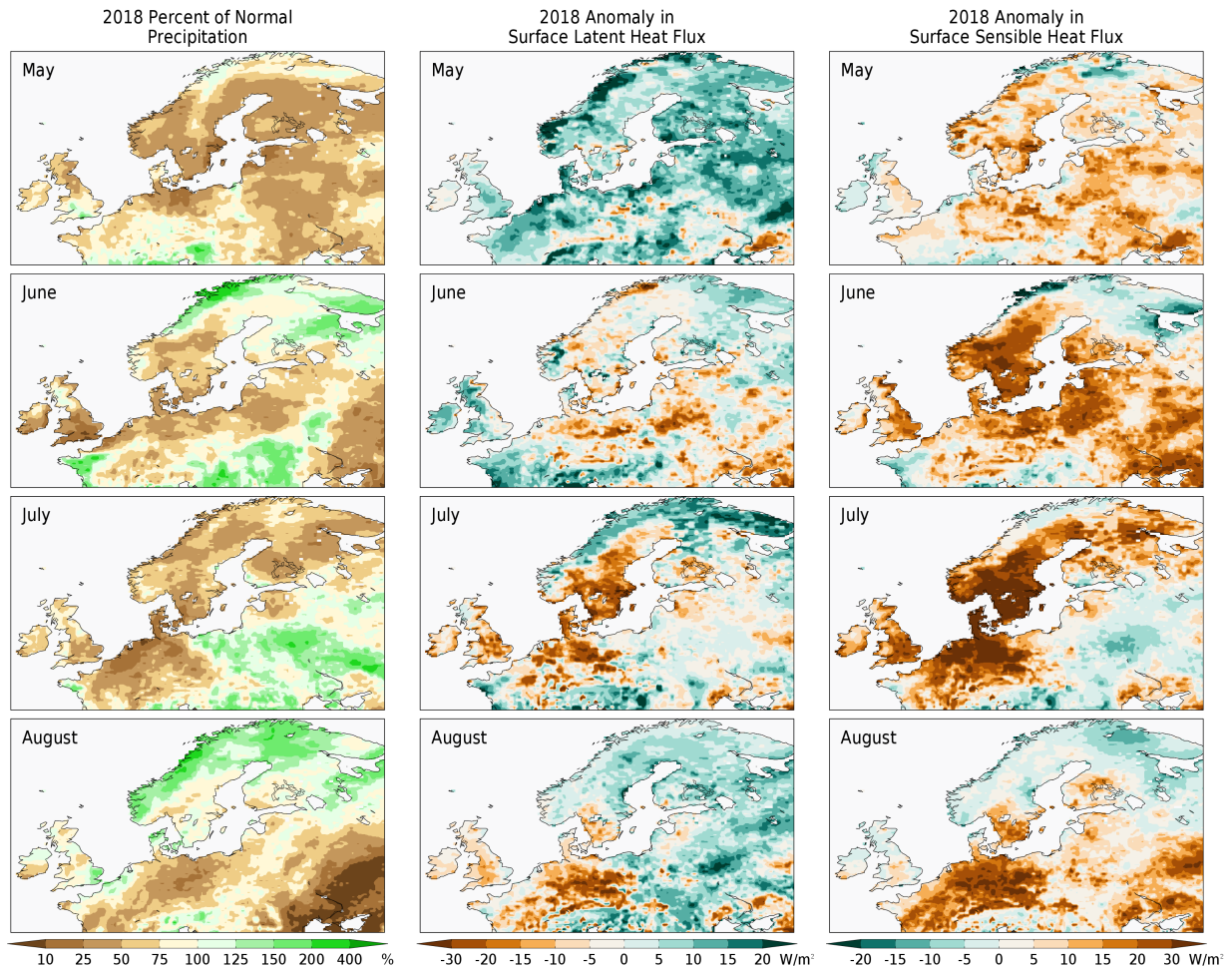


Figure S1: As in Figure 4, for monthly anomalies in precipitation (left column, as a percentage of normal for each month); surface latent heat flux (middle column) and surface sensible heat flux (right column).

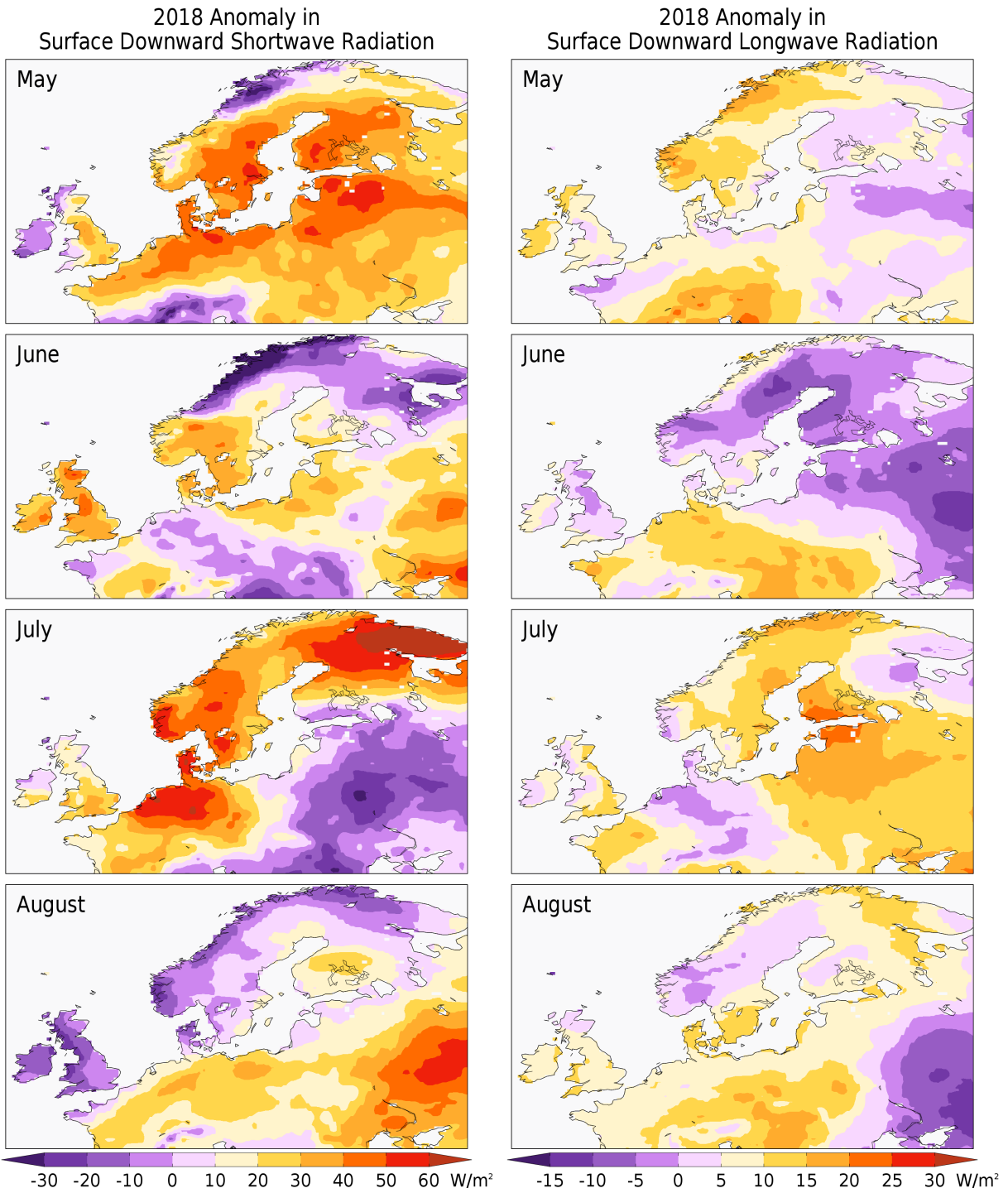


Figure S2: As in Figure 4, for monthly anomalies in surface downward shortwave radiation (left column) and surface downward longwave radiation (right column).

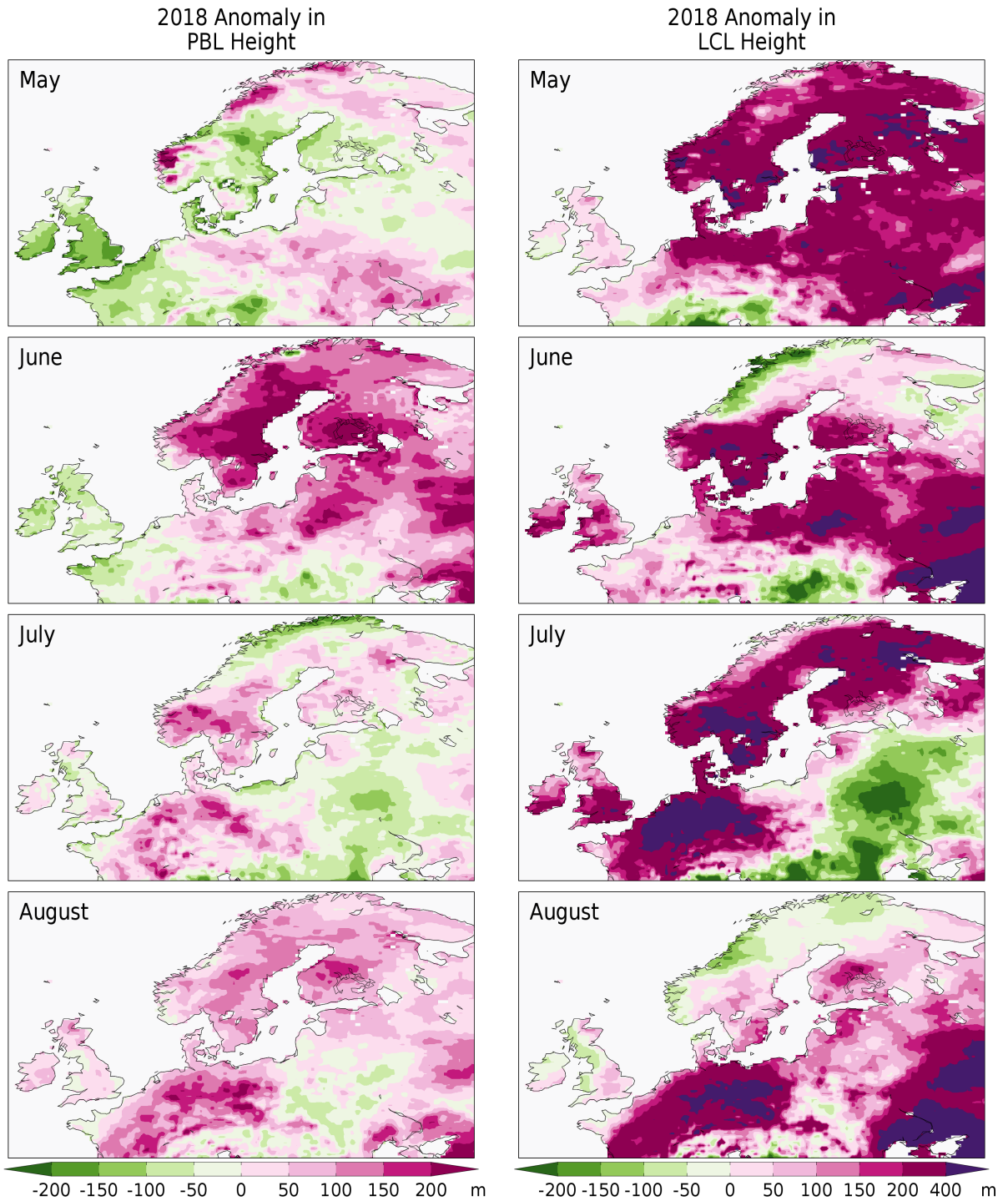


Figure S3: As in Figure 4, for monthly anomalies in daily mean ERA5 diagnostic planetary boundary layer height (left column) and daily mean lifted condensation level (right column).

MJJA 2018 Britain (vs. 1979-2017 Mean)

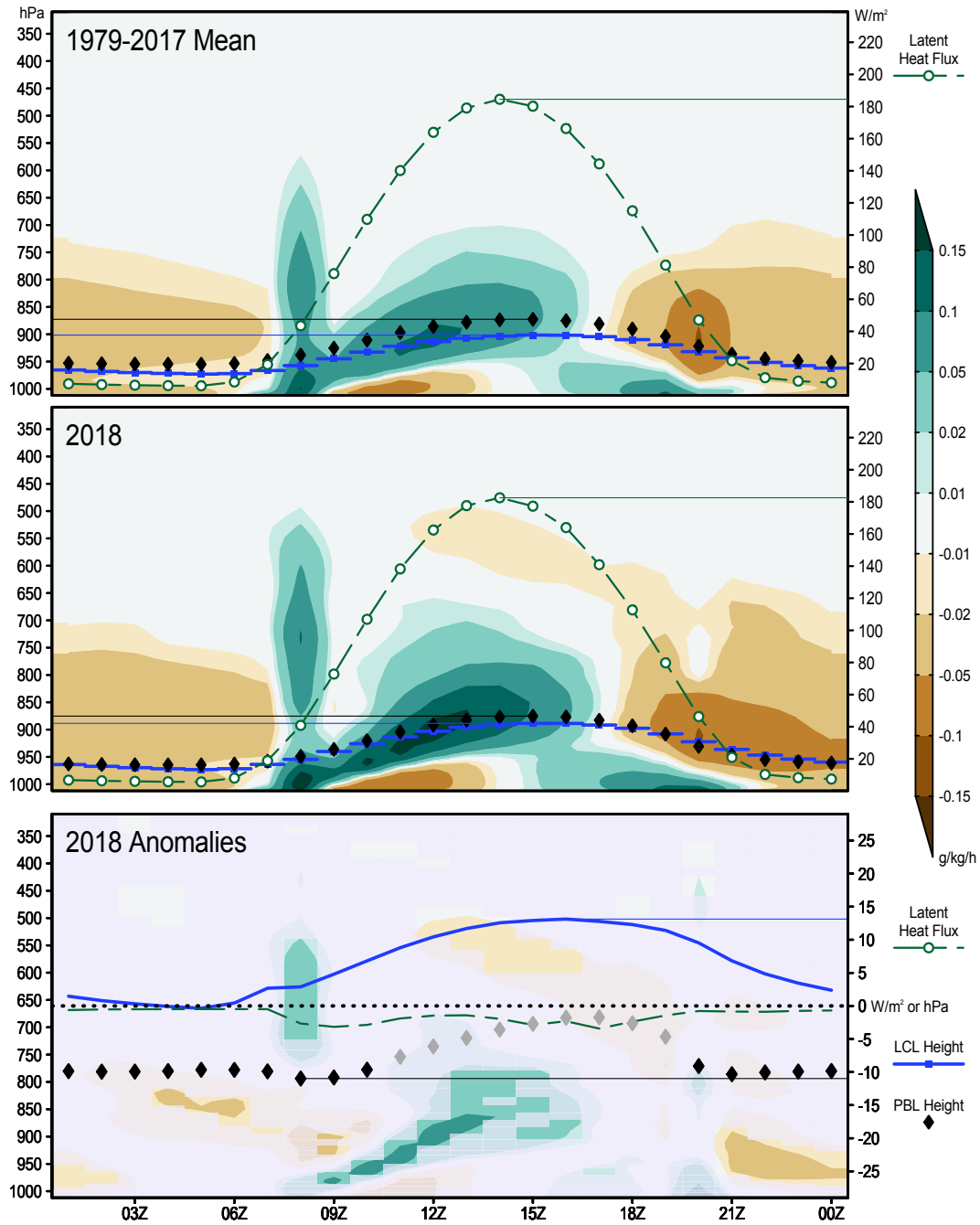


Figure S4: As in Figure 8 for moisture budget terms. Shading is for changes in water vapor content (specific humidity), and the lines and/or symbols are as indicated. Peculiar vertical features around 08 and 20UTC are artifacts of the 12-hour data assimilation cycle.

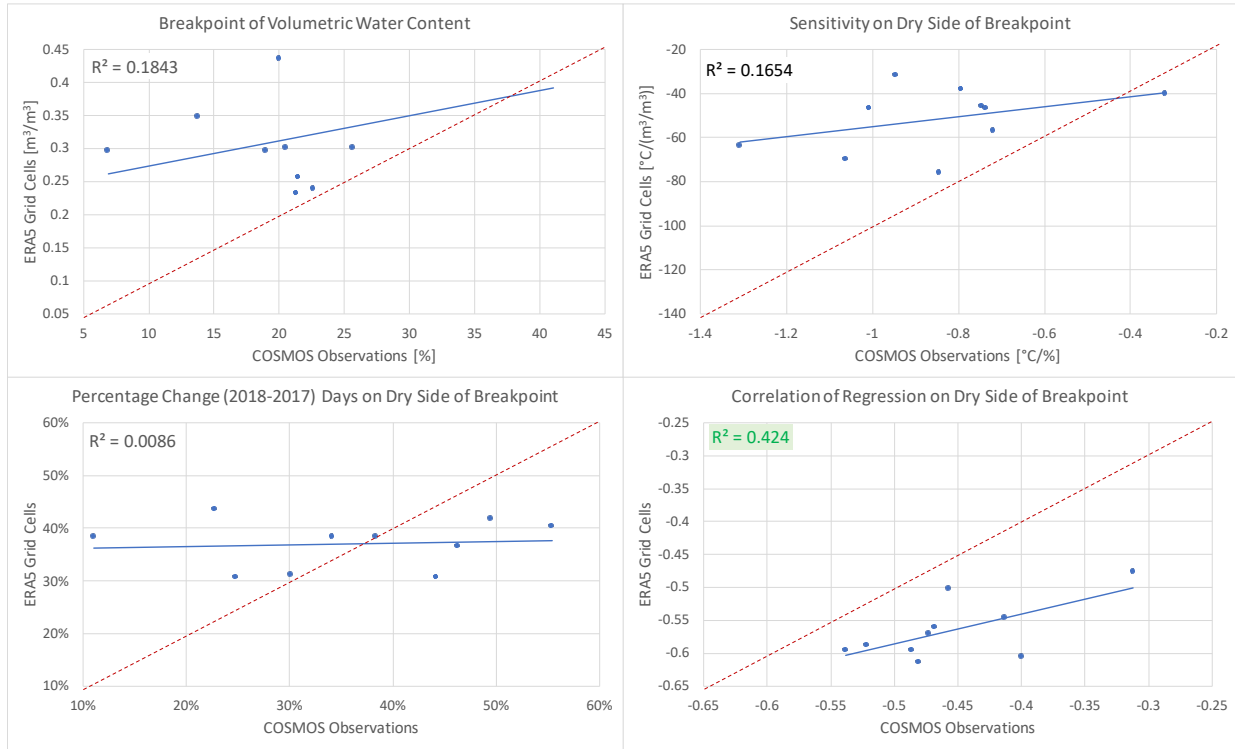


Figure S5: Comparison of selected breakpoint statistics between COSMOS stations and ERA5 grid cells containing each station; The estimated value of near-surface volumetric soil water content at the breakpoint (upper left); the increase in the number of dry days in 2018 compared to 2017 (lower left), the slope of the regression of daily maximum temperature on volumetric soil water content on the dry side of the breakpoint (upper right); and the correlation of that regression (lower right). In each panel, the dotted red line represents $X=Y$, perfect agreement between COSMOS and ERA5 data. The R^2 value shows the goodness of fit of the blue line to the points.

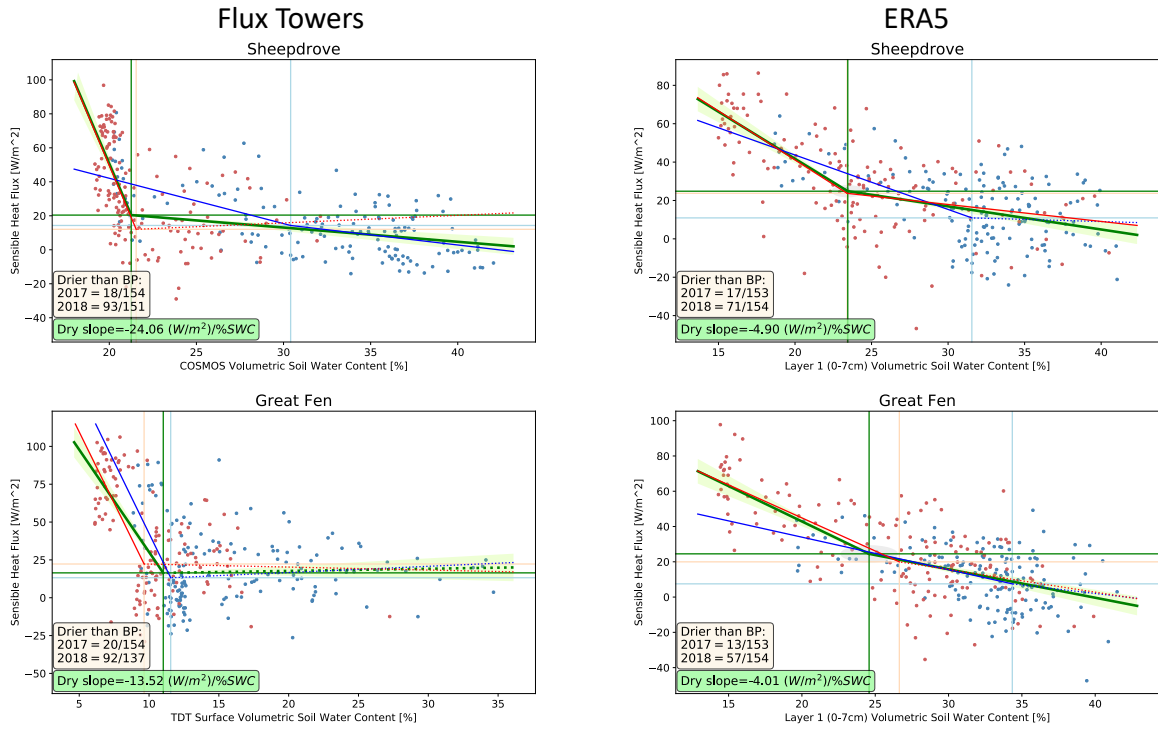


Figure S6: As in Figure 11 for sensible heat flux as the dependent variable.

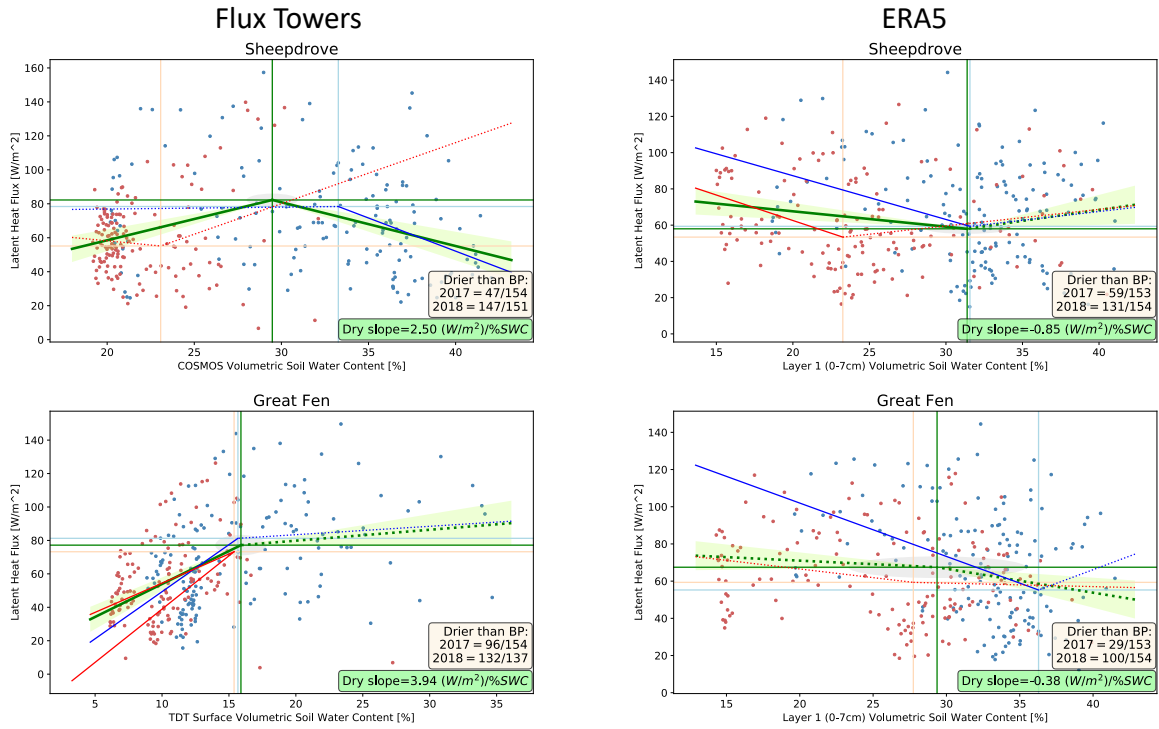


Fig S7: As in Figure 11 for latent heat flux as the dependent variable.

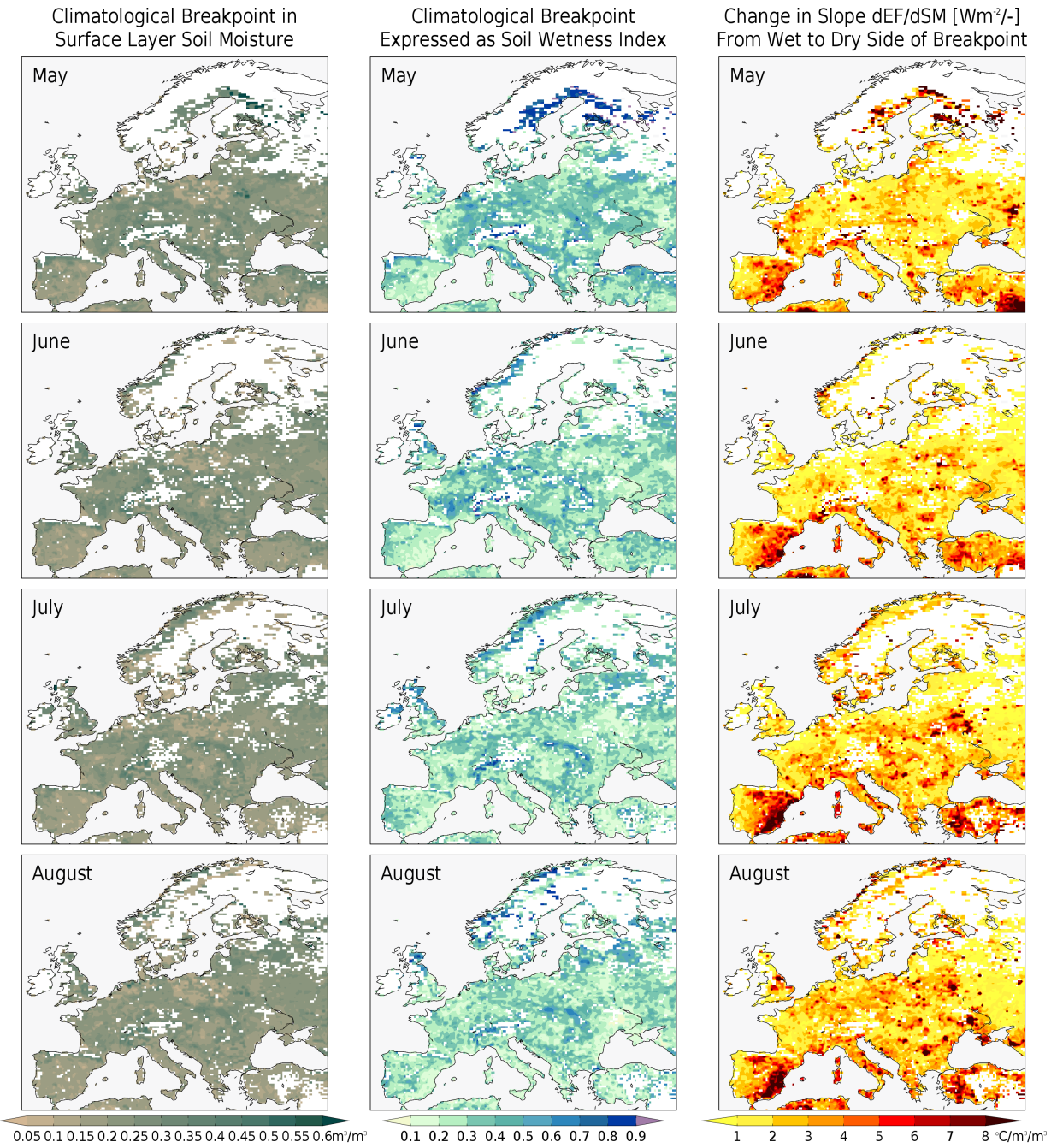


Fig S8: As in Figure 6 for breakpoint of evaporative fraction (EF) versus volumetric soil moisture.